**Technical Report on the Experimental
Microwave Thruster**

Roger J. Shawyer

September 2002 Issue 2

Prepared for:

SMART Feasibility Study Ref. 931
SBS South East
Department of Trade and Industry.

Contents

SPR Ltd

1. **Introduction**

This report documents the theoretical and experimental work carried out on a new concept of electrical propulsion for spacecraft. As this technology provides direct conversion from electrical energy to thrust, without expelling propellant, the implications for the space industry are profound.

However these profound implications also give rise to some scepticism and over a number of years, considerable effort has been directed at answering the many questions that have been raised. The theory and test results that are presented in this report have therefore been independently reviewed. They offer what is believed to be a complete verification of the concept.

The work has been supported by the Department of Trade and Industry via a SMART feasibility study award. It is now planned to progress the technology by developing an Engineering Model of a spacecraft engine, which will undergo dynamic testing.

SPR Ltd

2.   Theory

Consider a beam of photons incident upon a flat plate perpendicular to the beam. Let the beam have a cross-sectional area A and suppose that it consists of n photons per unit volume. Each photon has energy hf and travels with velocity c, where h is Planck's constant and f is the frequency. The power in the incident beam is then

$$P_0 = nhfAc. \tag{1}$$

The momentum of each photon is hf/c so that the rate of change of momentum of the beam at the plate (assuming total reflection) is $2nhfA$. Equating this change of momentum to the force F_o exerted on the plate, we find

$$F_0 = 2nhfA = \frac{2P_0}{c}, \tag{2}$$

which is the classical result for the radiation pressure obtained by Maxwell (Ref 1). The derivation given here is based on Cullen (Ref 2). If the group velocity of the beam is v then the rate of change of momentum at the plate is $2nhfA(v/c)$, so that the force F_g on the plate is in this case given by

$$F_g = \frac{2P_0}{c}(v/c). \tag{3}$$

We now suppose that the beam enters a vacuum-filled waveguide. The waveguide tapers from free-space propagation, with wavelength λ_0, to dimensions that give a waveguide wavelength of λ_g and propagation velocity v_g . This is the group velocity and is given by

$$v_g = \frac{c}{\sqrt{\mu_r e_r}} \frac{\lambda_0}{\lambda_g}. \tag{4}$$

Then from (3) and (4) (with $\mu_r = e_r = 1$) the force on the plate closing the end of the waveguide is

$$F_g = \frac{2P_0}{c}(v_g/c) = \frac{2P_0}{c}\frac{\lambda_0}{\lambda_g}; \tag{5}$$

see Cullen (p.102 Eq. (15)).

Assume that the beam is propagated in a vacuum-filled tapered waveguide with reflecting plates at each end. Let the guide wavelength at the end of the largest cross-section be λ_{g1} and that at the smallest cross-section be λ_{g2}. Then application of (5) to each plate yields the forces

$$F_{g1} = \frac{2P_0}{c}\frac{\lambda_0}{\lambda_{g1}}, \qquad F_{g2} = \frac{2P_0}{c}\frac{\lambda_0}{\lambda_{g2}}.$$

SPR Ltd

Now $\lambda_{g2} > \lambda_{g1}$, due to the difference in cross-sectional area, and hence $F_{g1} > F_{g2}$. Therefore the resultant thrust will be

$$T = F_{g1} - F_{g2} = \frac{2P_0}{c}\left(\frac{\lambda_0}{\lambda_{g1}} - \frac{\lambda_0}{\lambda_{g2}}\right). \qquad (6)$$

We note that if the forces had been the mechanical result of a working fluid within the closed waveguide assembly, then the resultant force would merely introduce a mechanical strain in the waveguide walls. This would be the result of a closed system of waveguide and working fluid.

In the present system the working fluid is replaced by an electromagnetic wave propagating close to the speed of light and Newtonian mechanics must be replaced with the special theory of relativity. There are two effects to be considered in the application of the special theory of relativity to the waveguide. The first effect is that as the two forces F_{g1} and F_{g2} are dependent upon the velocities v_{g1} and v_{g2}, the thrust T should be calculated according to Einstein's law of addition of velocities given by

$$v = \frac{v_1 + v_2}{1 + (v_1 v_2)/c^2}.$$

The second effect is that as the beam velocities are not directly dependent on any velocity of the waveguide, the beam and waveguide form an open system. Thus the reactions at the end plates are not constrained within a closed system of waveguide and beam but are reactions between waveguide and beam, each operating within its own reference frame, in an open system.

Note that the components of the reflection forces in the tapered side walls, along the axis of propagation, will cancel out, leaving a hoop stress in the walls.

From (6) and (4) we find

$$T = \frac{2P_0}{c}\left(\frac{v_{g1}}{c} - \frac{v_{g2}}{c}\right),$$

where

$$v_{g1} = c\lambda_0/\lambda_{g1}, \qquad v_{g2} = c\lambda_0/\lambda_{g2}.$$

Applying the above addition law of relativistic velocities we obtain

$$T = \frac{2P_0}{c^2}\left(\frac{v_{g1} - v_{g2}}{1 - v_{g1}v_{g2}/c^2}\right) = \frac{2P_0 S_0}{c}\left(\frac{\lambda_0}{\lambda_{g1}} - \frac{\lambda_0}{\lambda_{g2}}\right), \qquad (7)$$

where the correction factor S_o is

SPR Ltd

$$S_0 = \left\{ 1 - \frac{\lambda_0^2}{\lambda_{g1}\lambda_{g2}} \right\}^{-1} .$$

The concept of the beam and waveguide as an open system can be illustrated by allowing the velocity of the waveguide to increase in the direction of the thrust, until a significant fraction of the speed of light is reached. Let v_w be the velocity of the waveguide. Then as each plate is moving with velocity v_w, the forces on the plates, given by equation 5, are modified as follows:

$$F_{g1} = \frac{2P_0}{c^2} \left(\frac{v_{g1} - v_w}{1 - v_{g1} v_w / c^2} \right) = \frac{2P_0}{c^2} v_{ga}$$

and

$$F_{g2} = \frac{2P_0}{c^2} \left(\frac{v_{g2} + v_w}{1 + v_{g2} v_w / c^2} \right) = \frac{2P_0}{c^2} v_{gb}$$

The thrust is then given by

$$T = \frac{2P_0}{c^2} \left(\frac{v_{ga} - v_{gb}}{1 - v_{ga} v_{gb} / c^2} \right) \tag{8}$$

Thus as the velocity of the waveguide increases in the direction of thrust, the thrust will decrease until a limiting velocity is reached when $T=0$. This limiting value of v_w is reached when $v_{ga} = v_{gb}$. If v_w is increased beyond the limiting value, the thrust reverses.

Returning to a stationary waveguide, we now let the waveguide include a dielectric-filled section at the smaller end of the taper and choose the dimensions to ensure a reflection-free transmission of the beam from the vacuum-filled section to the dielectric-filled section. Note that the reflection-free interface, with matched wave impedances , will ensure no forces are produced at the interface. We also suppose that the dielectric medium has $\mu_r = 1$. Then the velocity v_{g2} is replaced by

$$v_{g2} = c \frac{\lambda_d}{\sqrt{e_r}\lambda_{g2}} ,$$

where λ_d is the wavelength in the unbounded dielectric medium. It then follows that the thrust takes the form

SPR Ltd

$$T = \frac{2P_0 S_d}{c}\left(\frac{\lambda_0}{\lambda_{g1}} - \frac{\lambda_d}{\sqrt{e_r}\,\lambda_{g2}} \right), \qquad S_d = \left\{ 1 - \frac{\lambda_0 \lambda_d}{\sqrt{e_r}\,\lambda_{g1}\lambda_{g2}} \right\}^{-1}. \qquad (9)$$

We suppose that the composite waveguide is resonant at the frequency of the microwave beam and that the conductive and dielectric losses are such that there are Q return paths (each at power P_0). Then the total thrust is finally given by

$$T = \frac{2P_0 Q S_d}{c}\left(\frac{\lambda_0}{\lambda_{g1}} - \frac{\lambda_d}{\sqrt{e_r}\,\lambda_{g2}} \right). \qquad (10)$$

References

1. Maxwell J.C.
    A treatise on Electricity and Magnetism
    Ist edition (Oxford University Press 1873)
    P. 391

2. Cullen A.L.
    Absolute Power Measurement at Microwave frequencies
    IEE Proceedings Vol 99 part IV 1952
    P. 100

3. Design

3.1. Design Description

The conceptual design of the experimental thruster is given in fig 1. It uses a tapered waveguide and a cylindrical dielectric filled section resulting in dissimilar wave velocities at each end of the waveguide. Thus the rate of change of momentum as the wave is reflected from each end wall is different and hence different forces, designated F1 and F2 are produced. The waveguide assembly is designed to be resonant at the operating frequency and therefore the force difference is multiplied by the Q of the assembly, producing a useful resultant force on the thruster.

 The thruster uses a magnetron as a source of microwave energy which is fed to the thruster through a tuned waveguide assembly. The electromagnetic wave is launched from a slot in the side wall of the thruster and propagates with an increasing guide

SPR Ltd

wavelength (λg) towards the dielectric section. As the waveguide cross section decreases, the waveguide impedance also decreases, such that, with correct dimensions, the impedance at the dielectric boundary is the same on both sides. This ensures propagation continues within the dielectric section without reflection at the boundary.

The thruster was designed around a Siemens dielectric resonator type LN89/52B with a dielectric constant (e_r) of 38. An operating frequency of 2450 MHz was selected to allow a commercial 850 W magnetron to be used as a power source. A tapered circular waveguide was designed with TM01 as the dominant mode of propagation. A rectangular feed structure was used with a resonant slot selected for the input launcher. Input matching was achieved by feed length adjustment and a tuning screw. An annular choke in the feed, open to the EMC enclosure, provided a path for reflected power to a load mounted on the inside wall of the enclosure. Thruster resonance tuning was carried out by variation of the position of the end wall, using screw adjusters. Optimum impedance matching at the dielectric boundary was achieved by fine adjustment of the axial position of the dielectric section.

A diagram of the complete thruster module is given in fig 2. This shows the thruster feed and magnetron mounted within an EMC enclosure. The magnetron is cooled by a dc fan. The enclosure contains sufficient cooling air volume to enable the magnetron to be run for 50 sec periods without overheating. Two thermistors are used for temperature monitoring and a thermal cut out is used to provide high temperature warning.

Although the emc enclosure provides initial screening, as well as containment of the cooling air, it was necessary to house the data monitoring electronics in separate screened boxes. Also to reduce thermal buoyancy effects during test runs a second 'hermetic' enclosure was manufactured. (Note that although this significantly reduced leakage of heated air it could not be considered truly hermetic.)

Two power detectors were developed, one mounted inside the module enclosure (det 1) and one mounted inside the thruster itself (det 2). Det 1 measures the power reflected back into the enclosure due to any mismatch at the thruster/feed interface. Det 2 measures the power level developed inside the thruster resonant cavity.

Both detectors are of the voltage probe type with attenuators and germanium diodes. The probe length and attenuator values were optimised to keep the detected signals within predicted dynamic range whilst minimising the risk of arc damage. Note that very high field strengths exist within the thruster and it was necessary to mount det 2 in a secondary cavity to prevent arcing.

The detector signals are amplified in two stages, with offset and gain control. Passive integrator circuits are used to provide d.c. outputs and to minimise noise. Note that the raw detector signals consist of 50 Hz pulses of power, as the magnetron itself is powered from a half wave rectified high voltage power supply, running at mains frequency.

The battery to supply the cooling fan together with amplifier supplies and controls are mounted in a separate control and data unit as shown.

SPR Ltd

The data signals from power detectors and thermistor together with thrust data from the load cell or precision balances are converted to digital format and logged on a laptop computer where they can be stored in Excel spreadsheets.

3.2 Design Model

The basic geometry of the thruster is determined by a number of factors illustrated in fig 1.

Inspection of equation 9 shows that to maximise the resultant force, λg_1 should be reduced such that it approaches λ_0, whereas λg_2 and e_r should be maximised. The reduction of λg_1 will be limited by allowable wall 1 dimensions whilst the increase of λg_2 will be limited by the required margin before the cut off dimension for wall 2 is reached. The value of e_r will be a compromise between maximising permittivity whilst minimising the dielectric losses which are a factor in limiting the value of Q.

At the dielectric boundary:

$$Ztm_3 = \frac{\lambda_0}{\lambda g_3}\sqrt{\frac{\mu_0}{e_0}} = Ztm_2 = \frac{\lambda_d}{\lambda g_2}\sqrt{\frac{\mu_0\mu_r}{e_0 e_r}} \tag{11}$$

where Ztm_3 is the wave impedance on the air side of the boundary and Ztm_2 is the wave impedance of the dielectric.

Finally the overall electrical length of the thruster must be a multiple of $\lambda e/2$ where λe is the effective wavelength of the thruster. This effective wavelength will equate to different values of physical length throughout the waveguide assembly.

The overall geometry was defined by building a mathematical model of the thruster based on an Excel spreadsheet. The physical length was divided into 0.5mm sections and the guide wavelength calculated for each section. The electrical length for that section was calculated and the summation of the section electrical lengths calculated.

Thus variations of diameters, lengths and e_r could be modelled, with the target of achieving an overall electrical length equal to $n\lambda e/2$.

The model also allowed the operation to be modelled in TE11 and TE12 modes, the nearest unwanted modes. The design was optimised to avoid the possibility of any unwanted mode operation.

Once the main parameters had been determined and a suitable commercially available dielectric resonator identified, a tolerance analysis was carried out. The expected variations in operating frequency, mechanical dimensions and electrical properties were input into the model. This enabled the adjustment ranges for resonance tuning and dielectric matching to be determined.

SPR Ltd

After manufacture, the "as built" dimensions were input into the design model, and at a nominal frequency of 2450 MHz this became the reference model against which the operation of the thruster could be compared.

The "as built" data is given in fig 3.

Table 1 gives two sections of the design model for 2450 MHz operation. The first section shows the position of the tuning plate (wall1) for resonance. The second section of the model shows the dielectric boundary and gives the total electrical length calculation.

It can be seen that *n=3*.

An estimate of the Q for the resulting design is given based on the Q for a similar volume cylindrical resonator for the air filled section (Qa) and the specified Q for the dielectric resonator (Qd). A matched input feed was assumed.

Then $$\frac{1}{Q} = 2\left(\frac{1}{Qa} + \frac{1}{Qd}\right)$$ (12)

For Qa = 60,562

and Qd = 14,987

then Qe = 6,008

The mean thrust predicted for the experimental thruster is calculated from equation 10.

where Po = 850W e = 38

$\square_{g1}$ = 0.20182 $\square_{g2}$ = 0.02055

$\square_0$ = 0.12236 $\square_d$ = 0.01985

then mean thrust T = 16.9 mN
                              = 1.72 grms

3.3   Design verification

The initial tuning of the thruster was carried out using a 100mW crystal controlled source operating at 2450 mHz. The position of the dielectric was adjusted using three positioning screws to provide axial movement of the dielectric. Minimum reflection at the boundary was determined by adjusting the axial position to give maximum reading on det 2. The resulting position at a length of 127mm corresponds to the nominal 50 ohm impedance of the dielectric resonator (see table 1).

SPR Ltd

Measurement of the position of the tuning plate for overall resonance of the thruster was carried out using two narrow band crystal sources operating at 2451.113 MHz and 2432.113 MHz. The predicted resonance positions are given in the sections of the design models shown in tables 2 and 3.

Thus table 2 predicts a resonance position at length 37.5 mm for 2451.113 MHz.

Fig 4 shows the measured resonance position is at length 37.8 mm.

Table 3 predicts a resonance position at length 32mm for 2432.113 MHz.

Fig 5 shows the measured resonance position is at length 31.9 mm.

Fig 5 also shows the detector output when the same test was carried out at 2432.113 MHz with a copper disc short circuiting the air/dielectric boundary. No resonance was measured, clearly showing that the resonance was due to propagation through both air and dielectric sections of the thruster.

An estimate of the Q of the thruster can be obtained by the 3dB bandwiths of the resonance peaks in figs 4 and 5. These give approximate Q values of 5,900 for the 2432 MHz test and 2500 for the 2451 MHz test. Note that considerable variation in the measured Q values occurred due to the movement of the tuning plate causing variation in the contact resistance between plate and the cylindrical wall. The TM01 mode relies on axial currents flowing through this plate/wall contact and some variation in performance throughout the test programme was attributed to this effect.

Another cause of performance variation is illustrated in fig 6, which shows the outputs of det 1 and det 2 over a typical run. The variation in magnetron output as it rapidly heats up shows a typical dip in input power to the thruster accompanied by a peak in reflected power.

Nevertheless over the large number of test runs reported in the next section, the measured thrust will be seen to be close to that predicted in section 3.2.

SPR Ltd

Design for 2450 MHz TM01 mode					
Length (mm)	Int Diam (mm)	Guide w/l (mm)	Electrical length	Total elec length	wave imp (Ohms)
35	117.2	203.93	0.002452	0.171626	226.0
35.5	117.2	203.93	0.002452	0.174078	226.0
36	117.2	203.93	0.002452	0.17653	226.0
36.5	117.2	203.93	0.002452	0.178981	226.0 tuning plate position
37	117.2	203.93	0.002452	0.181433	226.0 for resonance
37.5	117.2	203.93	0.002452	0.183885	226.0
38	117.2	203.93	0.002452	0.186337	226.0
38.5	117.2	203.93	0.002452	0.188789	226.0
39	117.2	203.93	0.002452	0.19124	226.0
39.5	117.2	203.93	0.002452	0.193692	226.0
40	117.2	203.93	0.002452	0.196144	226.0
125	95.1	745.37	0.000671	0.534383	61.8
125.5	94.9	779.49	0.000641	0.535024	59.1
126	94.8	818.92	0.000611	0.535635	56.3
126.5	94.7	865.19	0.000578	0.536213	53.3
127	94.6	920.53	0.000543	0.536756	50.1 dielectric starts
127.5	94.5	1014.54	0.000493	0.537249	45.4
128	94.3	1145.59	0.000436	0.537685	40.2
128.5	94.2	1346.69	0.000371	0.538057	34.2
129	94.0	1715.44	0.000291	0.538348	26.9
129.5	93.9	2803.62	0.000178	0.538526	16.4
130	93.7				

Electrical length for dielectric@   2450   Mhz =   1.1436

        Total electrical length for resonance =   1.1436
                                                    +   0.536756
                                                    -    0.178981
                                                         1.501375

Table 1. Design Model For 2450 Mhz

SPR Ltd

Design for 2451.113MHz TM01 mode					
Length (mm)	Int Diam (mm)	Guide w/l (mm)	Electrical length	Total elec length	wave imp (Ohms)

Length (mm)	Int Diam (mm)	Guide w/l (mm)	Electrical length	Total elec length	wave imp (Ohms)	
35	117.2	203.40	0.002458	0.172076	226.5	
35.5	117.2	203.40	0.002458	0.174534	226.5	
36	117.2	203.40	0.002458	0.176992	226.5	
36.5	117.2	203.40	0.002458	0.179451	226.5	
37	117.2	203.40	0.002458	0.181909	226.5	
37.5	117.2	203.40	0.002458	0.184367	226.5	tuning plate position
38	117.2	203.40	0.002458	0.186825	226.5	for resonance
38.5	117.2	203.40	0.002458	0.189284	226.5	
39	117.2	203.40	0.002458	0.191742	226.5	
39.5	117.2	203.40	0.002458	0.1942	226.5	
40	117.2	203.40	0.002458	0.196658	226.5	
125	95.1	714.25	0.0007	0.536561	64.5	
125.5	94.9	744.06	0.000672	0.537233	61.9	
126	94.8	778.06	0.000643	0.537876	59.2	
126.5	94.7	817.35	0.000612	0.538487	56.4	
127	94.6	863.44	0.000579	0.539066	53.4	dielectric starts
127.5	94.5	939.45	0.000532	0.539599	49.0	
128	94.3	1040.41	0.000481	0.540079	44.3	
128.5	94.2	1183.81	0.000422	0.540502	38.9	
129	94.0	1410.95	0.000354	0.540856	32.7	
129.5	93.9	1856.82	0.000269	0.541125	24.8	
130	93.7	3609.60	0.000139	0.541264	12.8	
130.5	93.6	Cut off @ 2451.113 Mhz				

Electrical length for dielectric @   2451.113 Mhz =   1.1441

Total electrical length for resonance =   1.1441
                                      +   0.539066
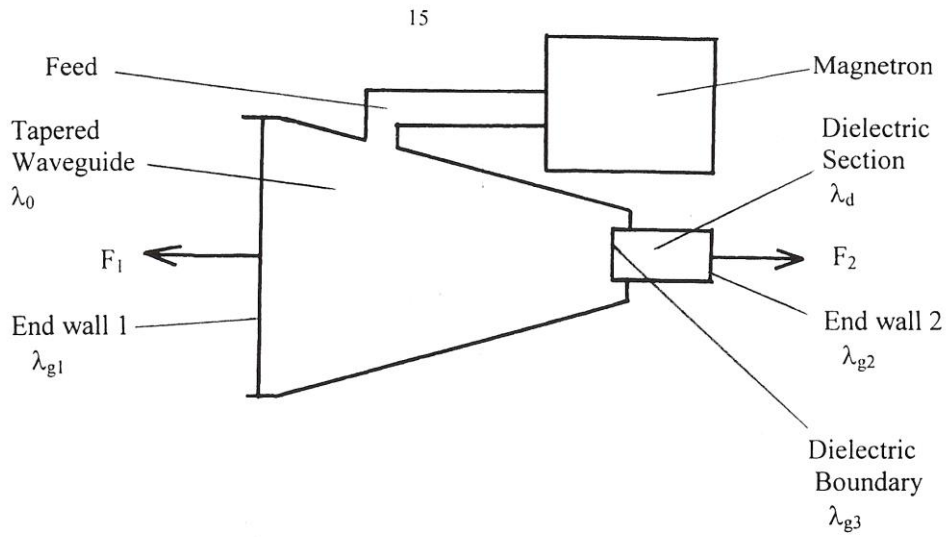   -   0.184367
                                          1.498799

Table 2.   Design Model For 2451 Mhz

SPR Ltd

Design for 2432.113 MHz TM01 mode					
Length (mm)	Int Diam (mm)	Guide w/l (mm)	Electrical length	Total elec length	wave imp (Ohms)
30	117.2	207.89	0.002405	0.144309	223.3
30.5	117.2	207.89	0.002405	0.146714	223.3
31	117.2	207.89	0.002405	0.149119	223.3
31.5	117.2	207.89	0.002405	0.151524	223.3
32	117.2	207.89	0.002405	0.15393	223.3 tuning plate position
32.5	117.2	207.89	0.002405	0.156335	223.3 for resonance
33	117.2	207.89	0.002405	0.15874	223.3
33.5	117.2	207.89	0.002405	0.161145	223.3
34	117.2	207.89	0.002405	0.16355	223.3
34.5	117.2	207.89	0.002405	0.165955	223.3
35	117.2	207.89	0.002405	0.168361	223.3
125	95.1	1038.23	0.000482	0.519762	44.7
125.5	94.9	1136.79	0.00044	0.520202	40.8
126	94.8	1270.64	0.000394	0.520595	36.5
126.5	94.7	1467.43	0.000341	0.520936	31.6
127	94.6	1799.40	0.000278	0.521214	25.8 dielectric starts
127.5	94.5	3152.92	0.000159	0.521373	14.7
128	94.3 Cut off @ 2432.113 Mhz				

Electrical length for dielectric @   2432.113 Mhz =   1.1346

    Total electrical length for resonance   =   1.1346
                                              +   0.521214
                                              -   0.15393
                                                  1.501884

Table 3. Design Model For 2432 Mhz

SPR Ltd

Feed

Tapered
Waveguide
λ_0

Magnetron

Dielectric
Section
λ_d

F_1

F_2

End wall 1
λ_{g1}

End wall 2
λ_{g2}

Dielectric
Boundary
λ_{g3}

Fig 1 Conceptual design of the experimental thruster.

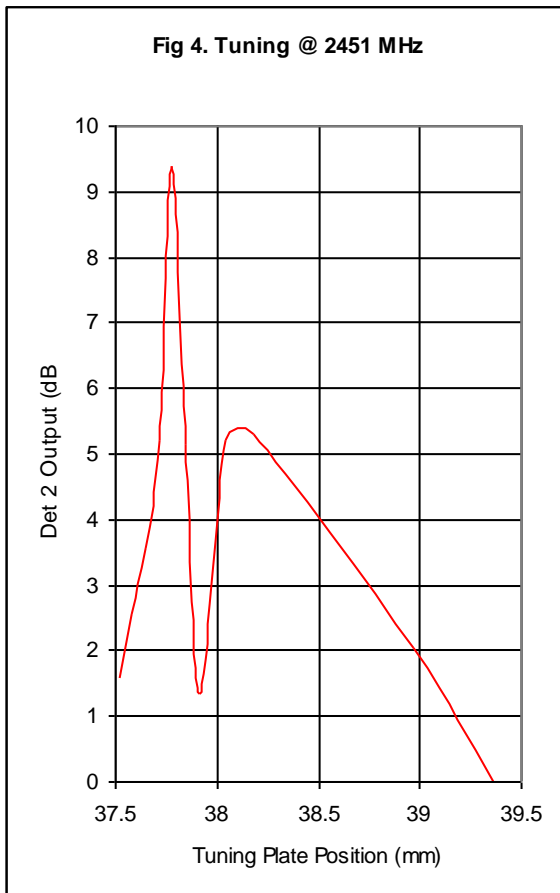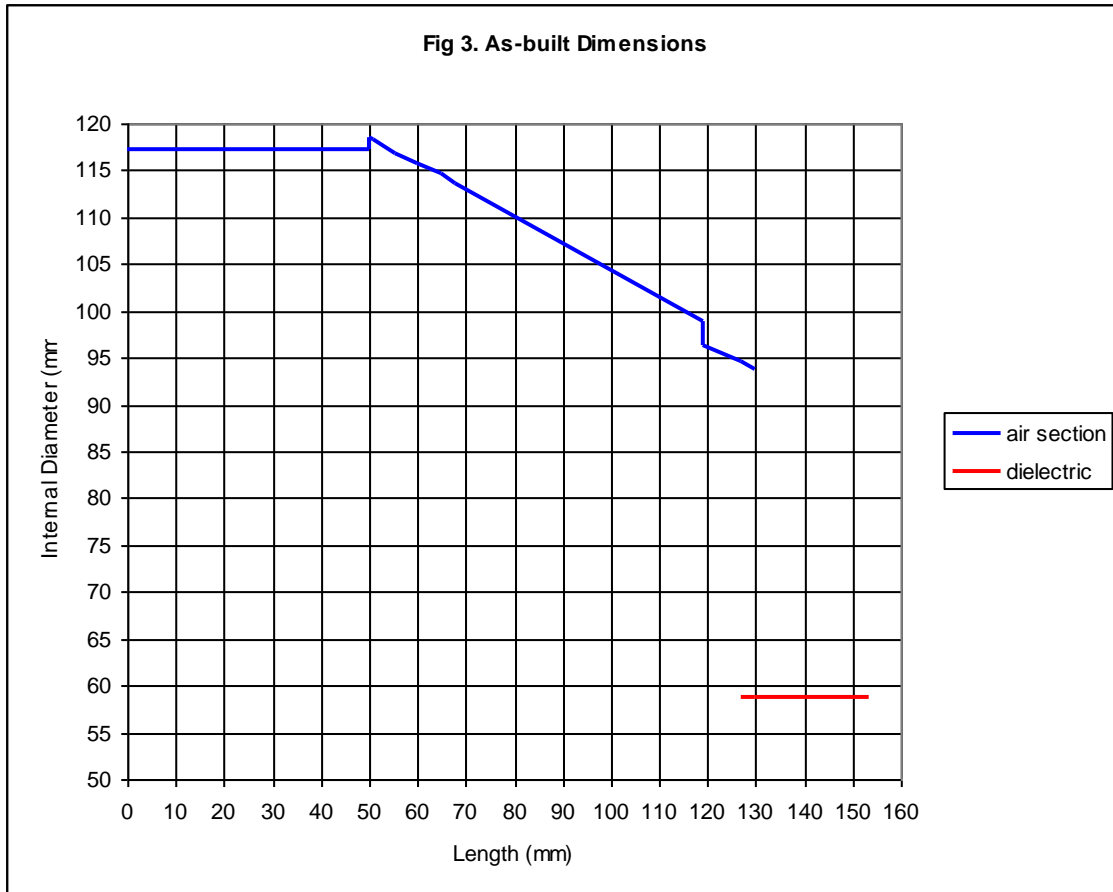Control & data
Unit

Computer
connector

Resonance
Tuning

Input tuning

EMC
enclosure

Det 1

Det 2

Reflected
power
load

H V
Connectors

Choke

Feed

Control
& data
Connector

Dielectric
Matching

Data
Amplifiers

Magnetron

Fan

Hermetic
enclosure
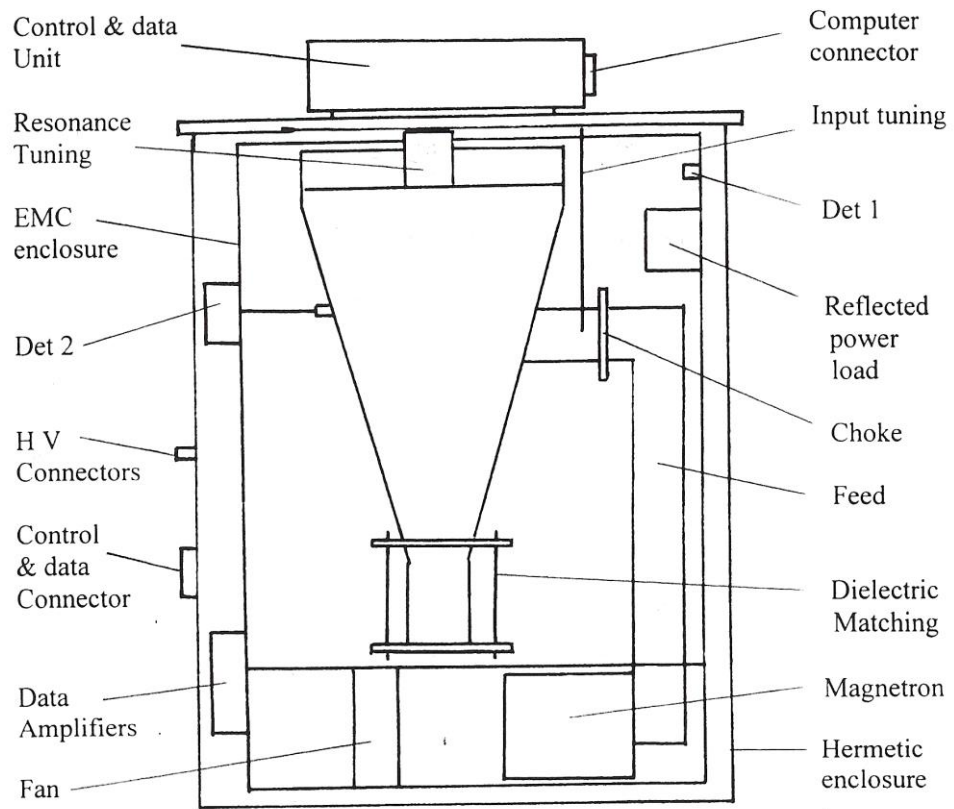
Fig 2. Diagram of the experimental thruster in nominal configuration

SPR Ltd

SPR Ltd

Fig 3. As-built Dimensions

Internal Diameter (mm)

- air section
- dielectric

Length (mm)

Fig 4. Tuning @ 2451 MHz

Det 2 Output (dB)

Tuning Plate Position (mm)

Fig 5. Tuning @ 2432 MHZ

Det 2 Output (dB)

- s/c dielect
- 2432 MHz

Tuning Plate Position (mm)

SPR Ltd

Fig 6 Input and Reflected Power

SPR Ltd
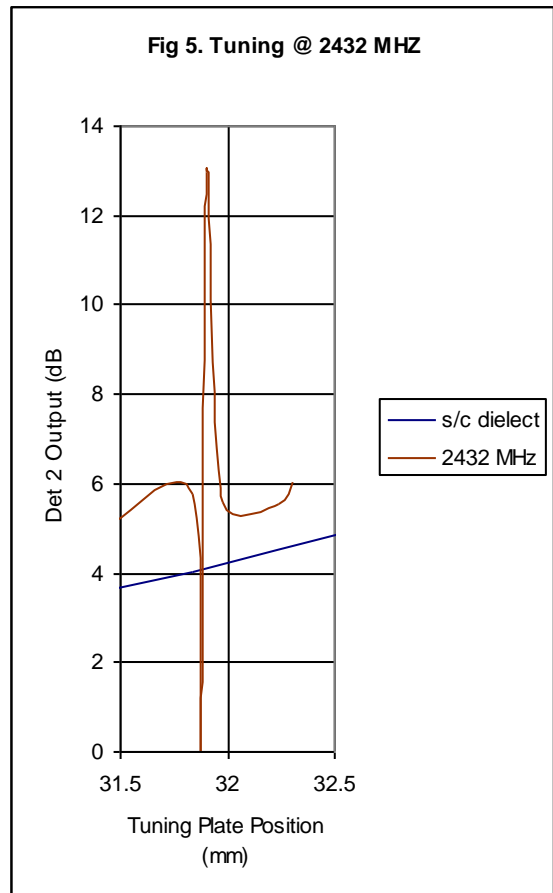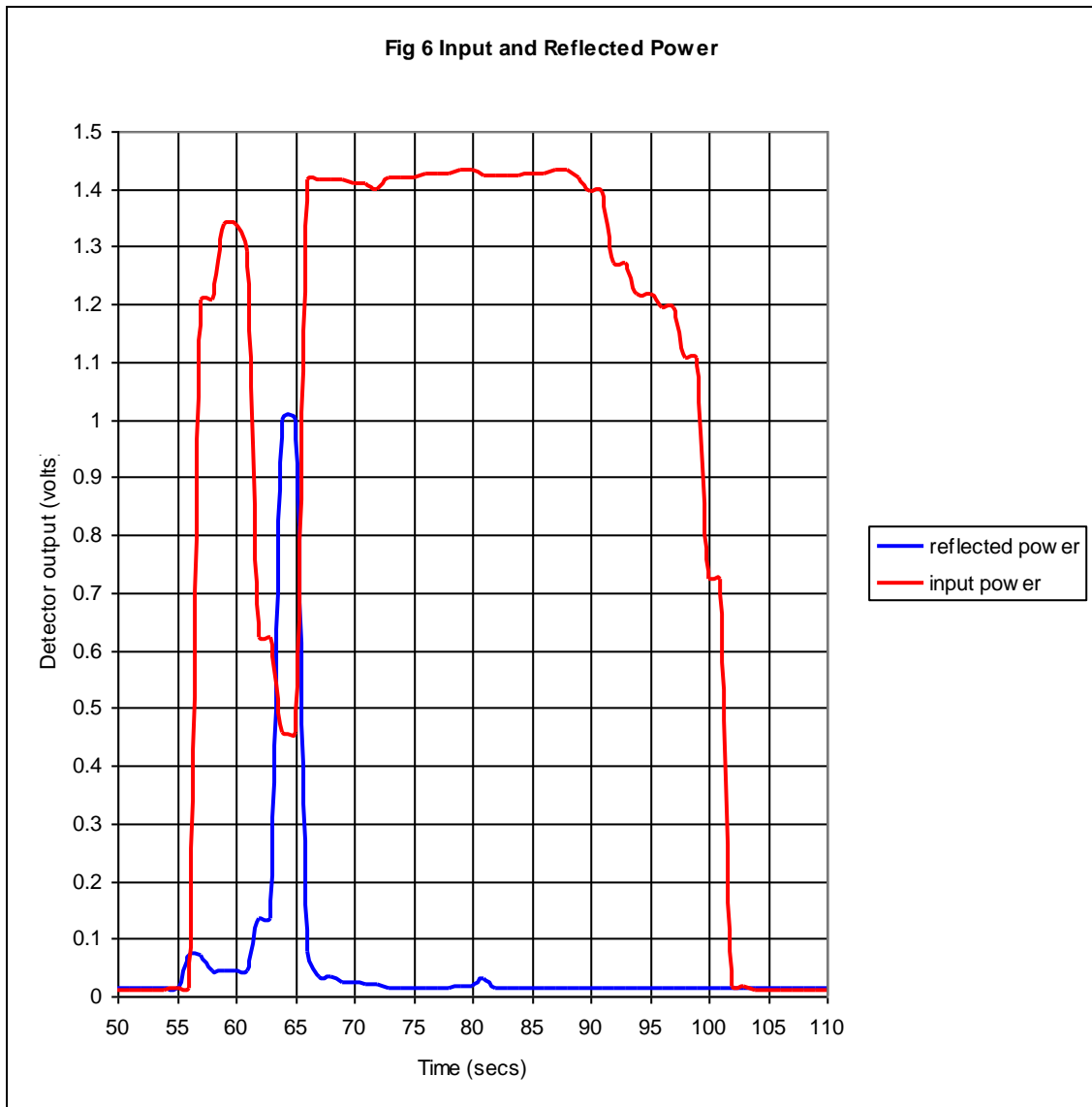
4. Test Programme

4.1 Load Cell Tests

The thruster module without the hermetic enclosure was mounted on a beam balance with the majority of the module mass being counterbalanced, as shown in Fig 7. The unbalanced mass was measured directly by a load cell connected to a digital meter via a low drift d.c. amplifier. Access to tuning plate adjustment and input tuning screw was at the top of the thruster module enclosure. The thruster module could be mounted in a nominal configuration(thrust direction up) or an inverted configuration (thrust direction down).

The magnetron was supplied with high voltage d.c. power from a half wave rectified power supply unit. The power was fed through three flexible links at the centre of the beam balance. The high cathode heater current (approximately 10A) necessitated multistrand links with consequent mechanical damping of any beam movement. Also the high current gave small but variable torques at the links when the magnetron was powered. Tests with a dummy load gave a mean force of + 30 mg with a standard deviation of 29 mg.

The load cell and amplifier contributed random noise to the results due to the high d.c. amplification required. Calibration tests gave a standard deviation of 20 mg with a calibration factor of 262 grms/volt.

For each test run, a test sequence of 50 secs off, 50 secs on and 50 secs off was adopted with load cell readings taken every 5 secs.

Three test runs were carried out for each test configuration or for each tuning variation. Fig 8 shows the results for three consecutive runs in nominal and inverted configurations, together with three consecutive runs in nominal configuration but with the thruster deliberately detuned to give zero thrust. The horizontal scale in fig 8 is 50 secs per division. Variable periods occurred between each run to allow the magnetron to cool.

The zero thrust run illustrates the thermal buoyancy effect due to heated air outgassing from the EMC enclosure as the thruster module heats up, resulting in a decrease in total mass.

The buoyancy effect can be calculated by adding the nominal and inverted test data and dividing by 2. This is also plotted in fig 8 and allowing for balance errors and run to run power variations, it is in good agreement with the zero thrust runs.

The peak thrust, averaged over the three nominal and inverted runs was 1.95grms. This appears in reasonable agreement with the thrust calculated in section 3.2. However the peak is achieved after a 50 sec run due to the time constant of the balance configuration. This is further investigated in section 4.4.

SPR Ltd

A total of 48 test runs were carried out in this series of tests, covering both nominal and inverted configurations over a range of input power and resonance tuning settings. Fig 9 shows the effect of the input tuning screw length on both input power, as measured on det 2 and thrust. Similarly Fig 10 gives input power and thrust measurements with variation in the position of the tuning plate. Note that it is possible to 'pull' the magnetron output frequency over a small tuning range and evidence of the double peak of the main lobe of the output spectrum of this type of commercial magnetron is seen.

The relationship between power and thrust is clearly demonstrated in these results, which were taken over separate test runs and power tests and included a change of magnetron.

4.2 Investigation of Spurious Effects

Having established thruster operation consistent with design expectations, attention was directed towards investigation of any spurious effects that may have the potential to produce similar test results. The effects considered were thermal, outgassing and electromagnetic. The test programme was carried out with constant settings for resonance and input tuning.

The major thermal effect is the change in buoyancy due to the heating of the air within the unit. A total air volume of 0.03 m^3 and a cooling fan is employed. This enables 50 secs of powered operation for 3 consecutive runs whilst limiting the maximum magnetron temperature to below 40º C. Actual air temperature rises were around 6º C per run, leading to thermal offset forces around 1 grm for the module test runs (see fig 8). This agrees with theoretical calculations for the displaced air mass.

Following the tuning test programme, the test set up was modified slightly to enable a rapid inversion of the unit to be achieved, and a dual test procedure was established. In this procedure, a single inverted run, at a given input and resonance setting, is followed by a nominal configuration run with the same settings. A typical result is given in fig 11, which is comparable to the runs given in fig 8 and illustrates that the sequence in which the test runs are carried out has no significance. Note also the deviations in slope during the early part of the 'on' periods due to the typical dip in magnetron power illustrated in fig 6.

Thermal expansion effects

Thermal expansion effects could change the effective centre of gravity of the unit, giving rise to spurious torque values on the balance. To eliminate this effect, inversion of the unit was achieved by a "front to back" rotation. This rotation maintains symmetry in the vertical axis and hence the centre line of thrust. (The mounting points at the top and bottom of the unit are carefully set to avoid movement from the vertical, following rotation.)

Thus spurious torques due to thermal expansion would be common to both nominal and inverted operation and no test data differences between configurations can be attributed to thermal expansion effects.

SPR Ltd

Note also that a later series of tests were carried out with the thruster directly mounted on a high capacity balance giving results in close agreement with predictions (see section 4.3). This confirms that the test data taken with the beam balance is not due to thermal expansion effects.

Cooling fan operation

To eliminate any spurious effects due to cooling fan operation, tests were carried out in a nominal configuration with both fan on and fan off. Fig 12 shows the results for a fan on-fan off-fan on, sequence of test runs.

It can be seen that rates of change of balance output during the heating phase (55 secs to 100 secs) and cooling phase (100 secs to 150 secs) are similar for all three runs and it is clear that there are no direct effects on the test data due to cooling fan operation.

Outgassing

The buoyancy effect occurs because the unit is not hermetically sealed, and the heated air expands with some outgassing. At the end of the powered operation the remaining higher temperature air gives a lower total mass.

It is important that the outgassing process itself does not produce spurious forces in a specific direction. To test for this effect, openings in the enclosure and panel edges were modified with plastic tape. Whilst not achieving a hermetic seal the modification would certainly have changed any significant directionality in the outgassing process.

Fig 13 compares the results of modified and unmodified runs. Rates of change of balance output are very similar for both runs. The peak negative output for the modified test is slightly less than for the unmodified test. This would be expected due to a lower total outgassed mass, resulting from the restricted outgassing path. The conclusion can be drawn that there is no directional component to the outgassing process.

Electromagnetic

With the high dc. currents being supplied to the magnetron cathode (approximately 10A) it was decided to eliminate any possibility of interaction with the Earth's magnetic field. Accordingly tests were carried out at zero degrees orientation (approximately North/South) and at 90 degrees orientation (approximately East/West). Fig 14 shows that within the normal spread of results no significant effect can be detected.
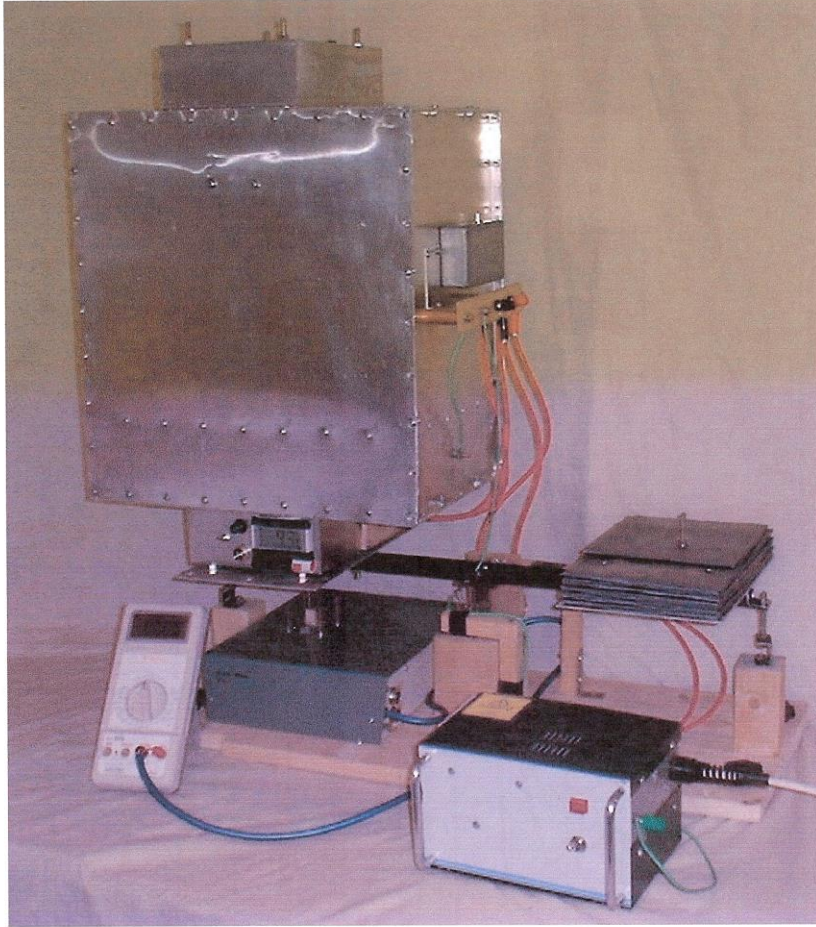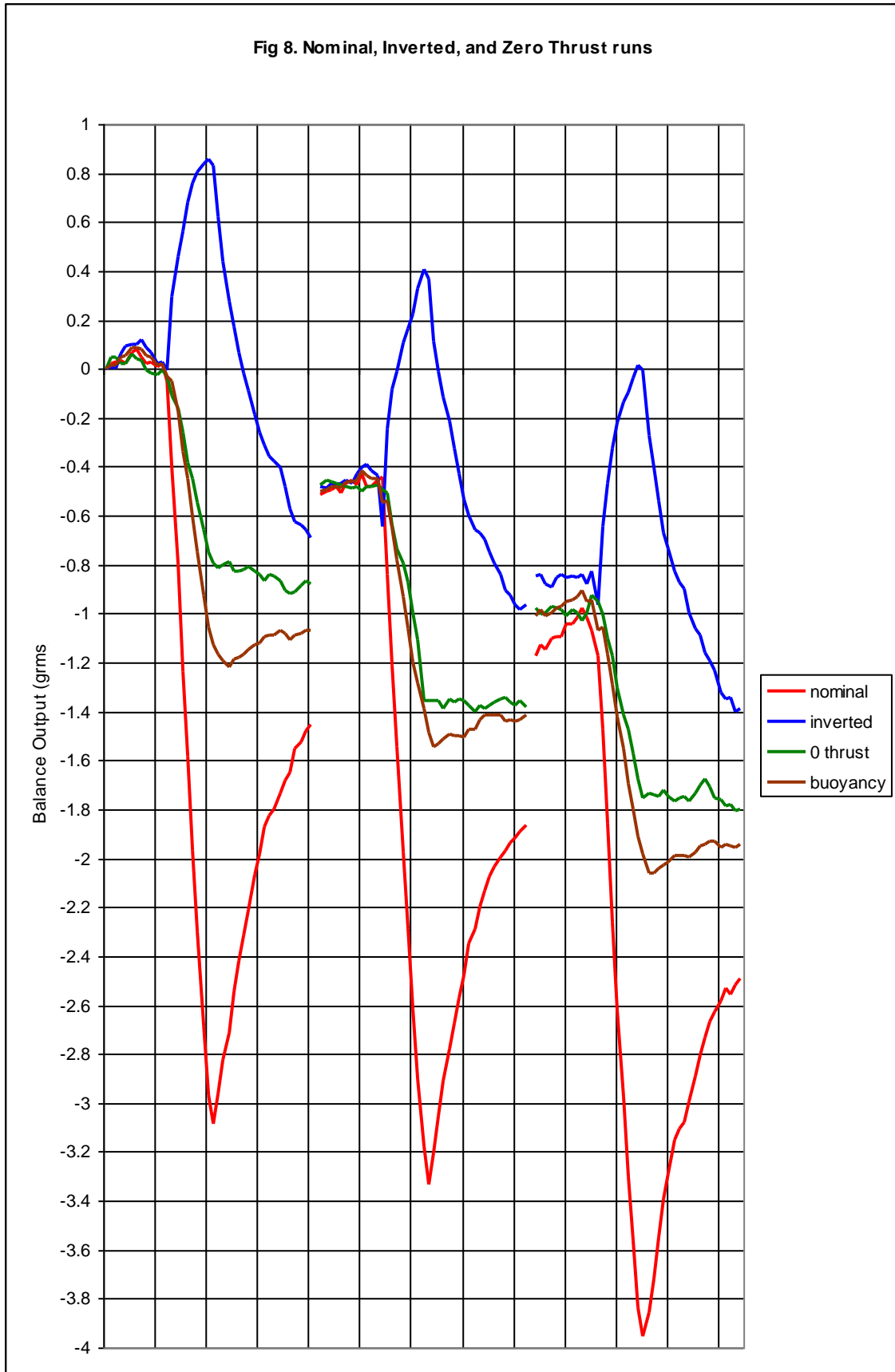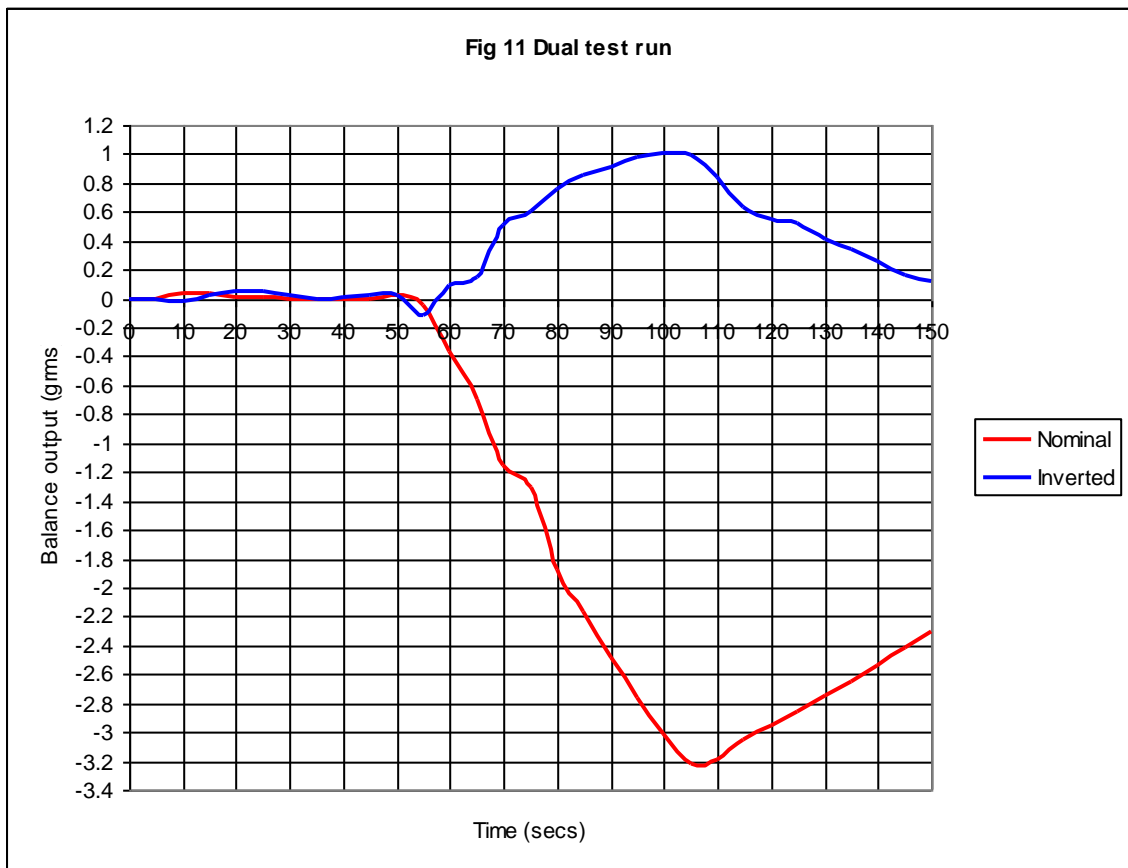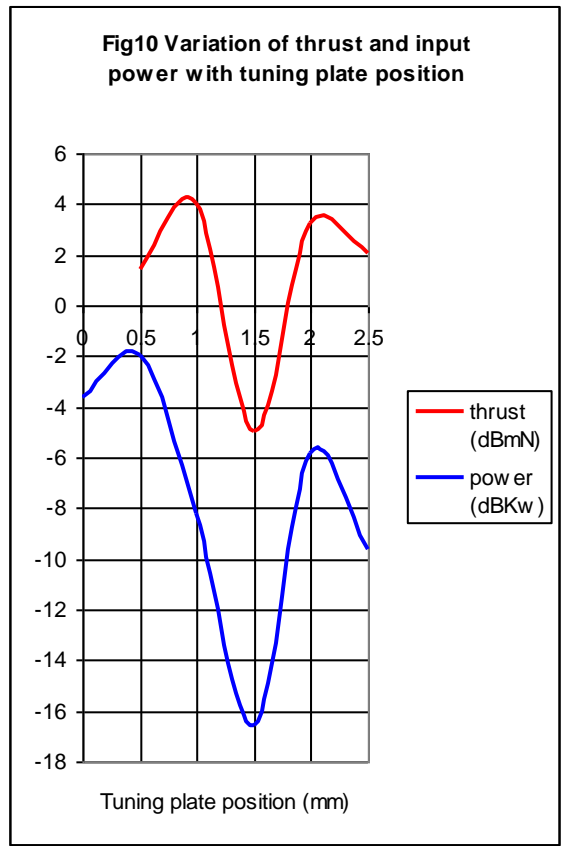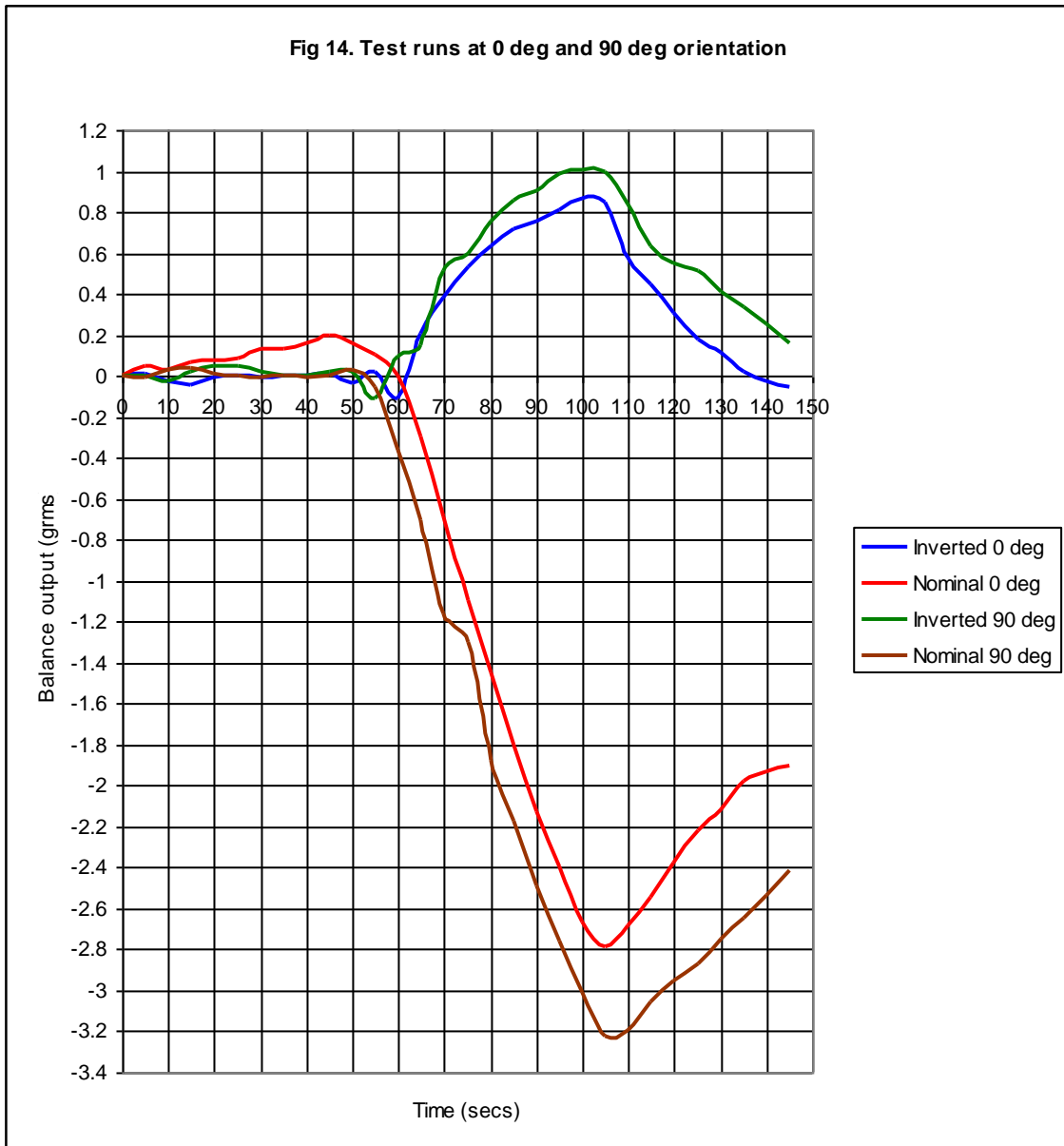
SPR Ltd

Fig 7 Thruster on beam balance with load cell

SPR Ltd

SPR Ltd

Fig 8. Nominal, Inverted, and Zero Thrust runs

SPR Ltd

Fig 9 Variation of thrust and input power with input tuning screw length

Fig10 Variation of thrust and input power with tuning plate position

Fig 11 Dual test run

SPR Ltd

Fig 12. Fan operation tests

Fig 13. Outgassing tests

SPR Ltd

Fig 14. Test runs at 0 deg and 90 deg orientation

SPR Ltd
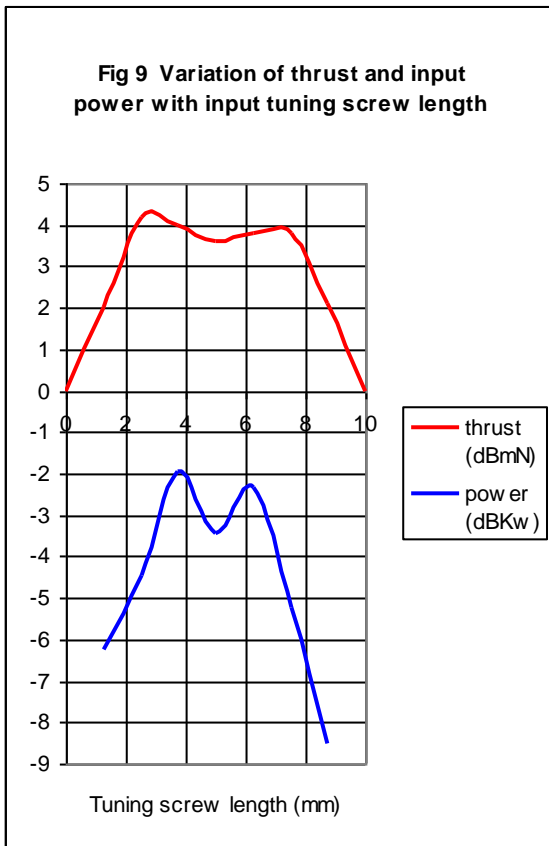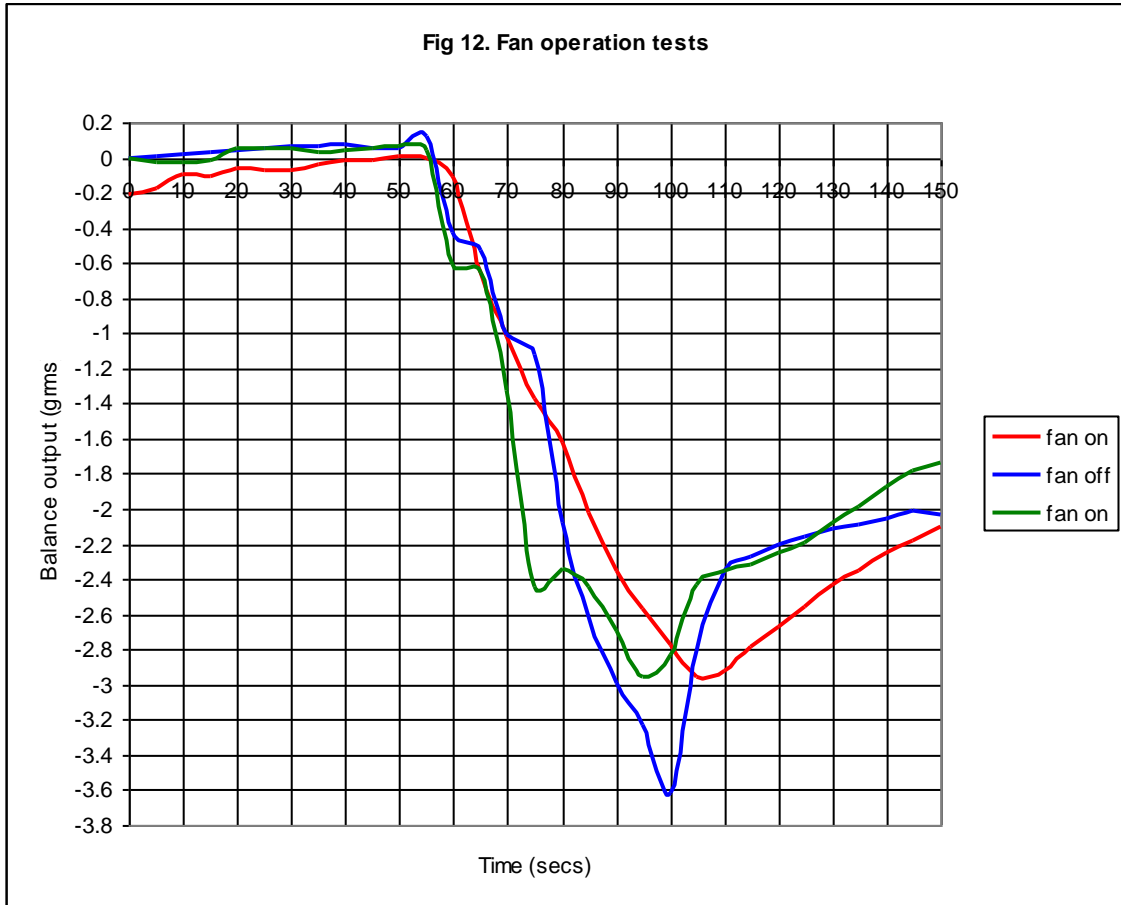
4.3 Precision Balance Tests

A further programme of tests was carried out using two precision balances.

In balance configuration 1, the thruster was mounted on a beam balance with 15.544 Kg of the thruster mass offset by a counterweight on the opposite side of the beam. The mass difference was measured on a 110 grm electronic balance with a resolution of 1 mgrm and a spring constant of 1.635×10^{3} N/m .

In balance configuration 2, the thruster was mounted directly on a 16 Kg electronic balance with a resolution of 100 mgrm and a spring constant of 1.825×10^{5} N/m . Fig 15 shows the thruster module complete with hermetic enclosure nominally mounted in balance configuration 2.

The object of the programme was to obtain results from a hermetically sealed thruster and to investigate the thrust profile seen during the test runs using the load cell.

4.3.1   Tests using the hermetic enclosure

Maintaining a hermetic seal using the enclosure, over a full test programme, proved difficult. However two sets of tests carried out in balance configuration 2 illustrate the results of minimising the buoyancy effect by significantly decreasing the outgassing of heated air.

Fig 16 gives results without the hermetic enclosure for nominal and inverted thruster configurations. Also given is a zero thrust result with the thruster deliberately detuned. Note that although the buoyancy effect gives a negative force of 1.4 grms, the positive and negative thrusts are only 0.2 grms.

Fig 17 gives results for the thruster inside the hermetic enclosure. For these tests a positive thrust of 0.4 grms after 20 secs power and a negative thrusts of 0.6 grms after 30 secs are achieved. A negative buoyancy force of 0.1 grms is identifiable for the detuned test run.

Figs 16 and 17 also clearly illustrate the much lower rate of thrust increase measured in balance configuration 2 compared to those measured in the load cell tests.

In contrast fig 18, which gives results in balance configuration 1 show higher thrust rates, and peak thrust values comparable to those obtained using the load cell. Fig 18 also illustrates the very much reduced buoyancy effect using the hermetic enclosure. This is calculated as the difference between the inverted and nominal test results.

4.3.2   Investigation of thrust/time profiles

The difference in the thrust/time profiles measured in balance configuration 1 and 2 is an important demonstration of the difference between measuring the thrust derived from a momentum exchange between electromagnetic wave and thruster end wall, and the forces that would be measured due to other spurious effects. To understand

SPR Ltd

this difference the theoretical basis of the energy exchange between the electromagnetic wave and the potential energy eventually stored in the spring within the balance was investigated.

Theory

The equation for the thrust output of the microwave thruster is given by equation 11:

$$T = \frac{2P_0 Q S_d}{c}\left(\frac{\lambda_0}{\lambda_{g1}} - \frac{\lambda_d}{\sqrt{e_r}\,\lambda_{g2}}\right)$$

Let D be the thruster design factor where

$$D = QS_d\left(\frac{\lambda_0}{\lambda_{g1}} - \frac{\lambda_d}{\sqrt{e_r}\,\lambda_{g2}}\right)$$

Then

$$T = \frac{2P_0 D}{c} \qquad\qquad (13)$$

Now the thrust is a result of the rate of change of momentum of the EM wave within the thruster.

Let R_e be the change of momentum of the EM wave over time t_m

Then from the basic equation   force = mass x acceleration :

$$T = \frac{R_e}{t_m}$$

thus $\qquad\qquad R_e = \frac{t_m 2P_0 D}{c} \qquad\qquad (14)$

For an unrestrained thruster the momentum transferred from the EM wave to the thruster is given by

$$R_m = MV \qquad\qquad (15)$$

where M is the mass of the thruster and V is the velocity attained in time t_m.

SPR Ltd

Then by the conservation of momentum

$$MV = \frac{t_m 2P_0 D}{c}$$

Thus the time to raise the velocity of the thruster by V is

$$t_m = \frac{MVc}{2P_0 D} \qquad (16)$$

However, if the thruster is restrained by a spring balance, the kinetic energy of the moving thruster is transferred to the potential energy stored in the spring as the spring is compressed.

This potential energy is given by:

$$E_p = \frac{Kl^2}{2} \qquad (17)$$

where K is the spring constant and l is the spring compression due to the energy transfer.

Now the apparent change in mass m displayed on the balance is the measured thrust T_m.

Thus $\quad m = \dfrac{T_m}{g}$

The kinetic energy stored in the spring at any time is therefore given by

$$E_k = \frac{T_m V^2}{2g} \qquad (18)$$

By conservation of energy

$$\frac{T_m V^2}{2g} = \frac{Kl^2}{2}$$

thus $\quad V = l\sqrt{\dfrac{Kg}{T_m}} \qquad (19)$

Now the time required to raise the velocity of the thruster by V is given in equation 16

SPR Ltd

From equations 16 and 17

$$t_m = \frac{Mcl}{2P_0 D} \sqrt{\frac{Kg}{T_m}} \, .$$ (20)

Experimental Thruster Operation

The experimental thruster is powered from a magnetron supplied by a 50 Hz half wave rectified voltage. The power of the EM wave within the thruster is therefore a pulse waveform with 10 msec pulses of $\sin^2 x$ shape, at a repetition rate of 50 pulses per sec. This is illustrated in the oscilloscope trace of the output from a power detector mounted within the thruster given in fig 19.

This pulsed thrust produces a balance response which modifies each pulse by the time required to achieve energy transfer t_m msecs and by the mechanical time constant of the balance itself.

Let the peak thrust in each pulse be T_p and the damped balance time constant be t_b msecs.

Then in the 10 msec pulse period from $t = 0$ to $t = 10$

$$T = T_p \left(\frac{t}{t_m} \right) \left(1 - e^{\frac{-t}{t_b}} \right) \sin^2 \pi \frac{t}{10} \, .$$ (21)

During the interpulse period from $t = 10$ to $t = 20$

$$T = T_{10} e^{-\left(\frac{t-10}{t_b} \right)}$$ (22)

where T_{10} is the measured value of thrust at 10 msecs.

After 20 msecs the cycle repeats with T for the next cycle being added to the residual value of T from the first cycle.

The solution to equations 21 and 22 is given in fig 20 for the first two cycles of a test run in balance configuration 1.

Thus for a test run of hundreds of cycles the measurement of thrust will increment towards the peak thrust T_p with the rate of increment dependent on the mass of thruster and the spring constant.

SPR Ltd

Comparison of predicted thrust/time profile with test results

For the experimental thruster the RMS power input (P_0) is 850W, the design factor (D) is 2470 and the mass (M) is 15.59 Kg.

From equations 21 and 22 the thrust profiles for balance configurations 1 and 2 were calculated .

In fig 21 these predictions are compared to the thrust data taken over 25 seconds of test runs in balance configurations 1 and 2.

In a normal test run the power is on for 50 secs. In the first 5 to 15 secs the cathode is heating up prior to microwave power being produced. Over the next 10 secs the rapid temperature rise of the magnetron itself causes frequency instability giving rise to the variation in output power illustrated in fig 6. At the end of the 50 sec period the magnetron is reaching its maximum operating temperature, causing further frequency instability. There is therefore, typically 25 secs of stable thruster operation during a test run.

Fig 21 shows that over this 25 sec period there is close agreement between the predicted and the measured results in both balance configuration 1 and balance configuration 2.

4.3.3.   Further Consideration of spurious forces

If the force measured on the balance had been due to a constantly applied force (e.g. a mass change) then the balance response would merely follow the balance time constants. Before test runs, the balances are calibrated by adding precision weights. The scaled calibration responses are given in figs 22 and 23 together with the predicted responses using the balance time constants. Allowing for the balance oscillations that occur experimentally, the predicted and calibration responses agree closely.

Similarly if the force measured on the balance had been due to a linear change in the mass (e.g. due to thermal effects) the responses would be the linear change modified by the balance time constants illustrated in fig 24.

Inspection of figs 22,23 and 24 show that in each case of an applied force due to a spurious effect, the predicted responses of the two balance configurations are quite different to the response due to a thruster output of equation 10. Specifically, for each spurious force, the rate of increase in predicted force is higher for configuration 2 than for configuration 1. However for the measured thruster output given in fig 21 the rate of increase in thrust is higher for configuration 1 than for configuration 2.

It is instructive to consider what the balance responses would be for a pulsed force waveform rather than for the pulsed momentum produced by the thruster. Such a force waveform could occur if there were a spurious pulsed electromotive force present rather than the thruster output, given by equation 10.

SPR Ltd

Let this peak force be equal to the apparent change in mass m times gravitational acceleration g.

The potential energy stored in the spring balance for an applied force is given by

$$E_p = mgl \tag{23}$$

thus by conservation of energy

$$mgl = \frac{Kl^2}{2} \tag{24}$$

Now compression l is given by:

$$l = Vt_f$$

Where t_f is the time for the force to achieve compression l and velocity V is given by:

$$V = gt_f$$

then substituting in equation 24 gives

$$t_f = \sqrt{\frac{2m}{K}} \tag{25}$$

Applying t_f to equations 21 and 22 in place of t_m gives predicted responses for the two balance configurations and is shown in fig 25.

Once again, the rate of increase in the predicted force is higher for configuration 2 than it is for configuration 1,which is opposite to that measured for the thruster and given in fig 21.
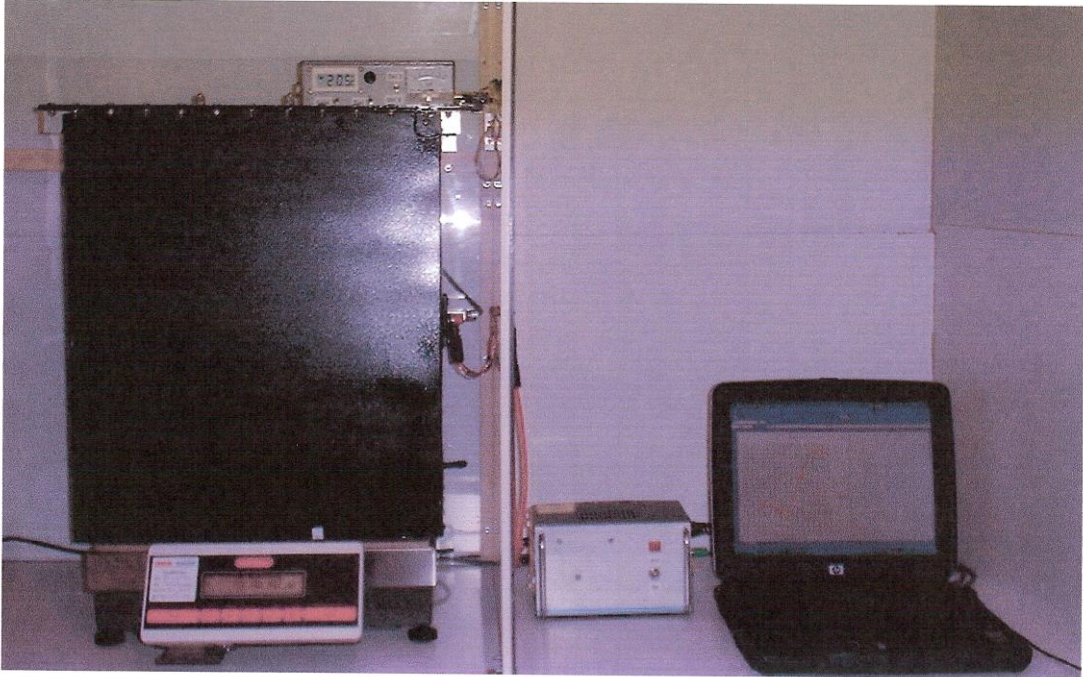
SPR Ltd

Fig 15. Thruster with hermetic enclosure in balance configuration 2.

SPR Ltd

SPR Ltd

Fig 16.Configuration 2 tests without hermetic enclosure

SPR Ltd

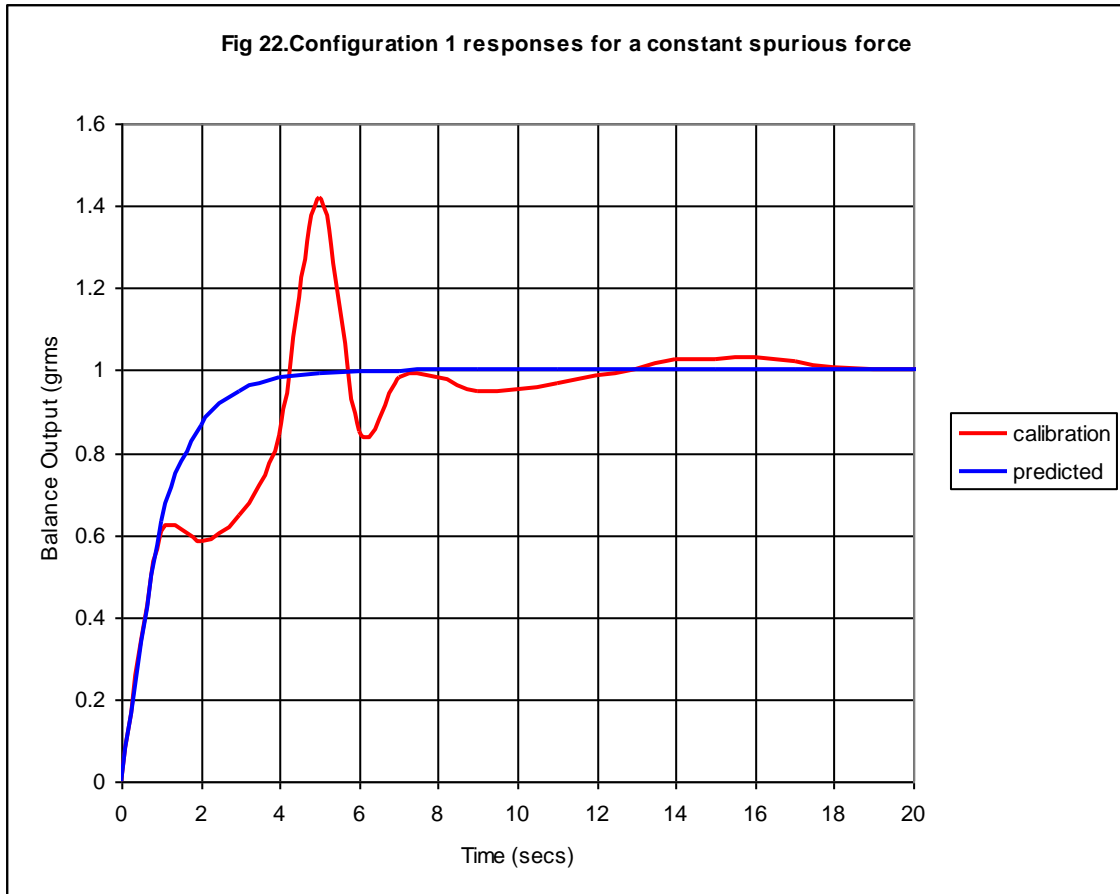Fig 17.Configuration 2 tests with hermetic enclosure

Fig 18. Configuration 1 tests with hermetic enclosure
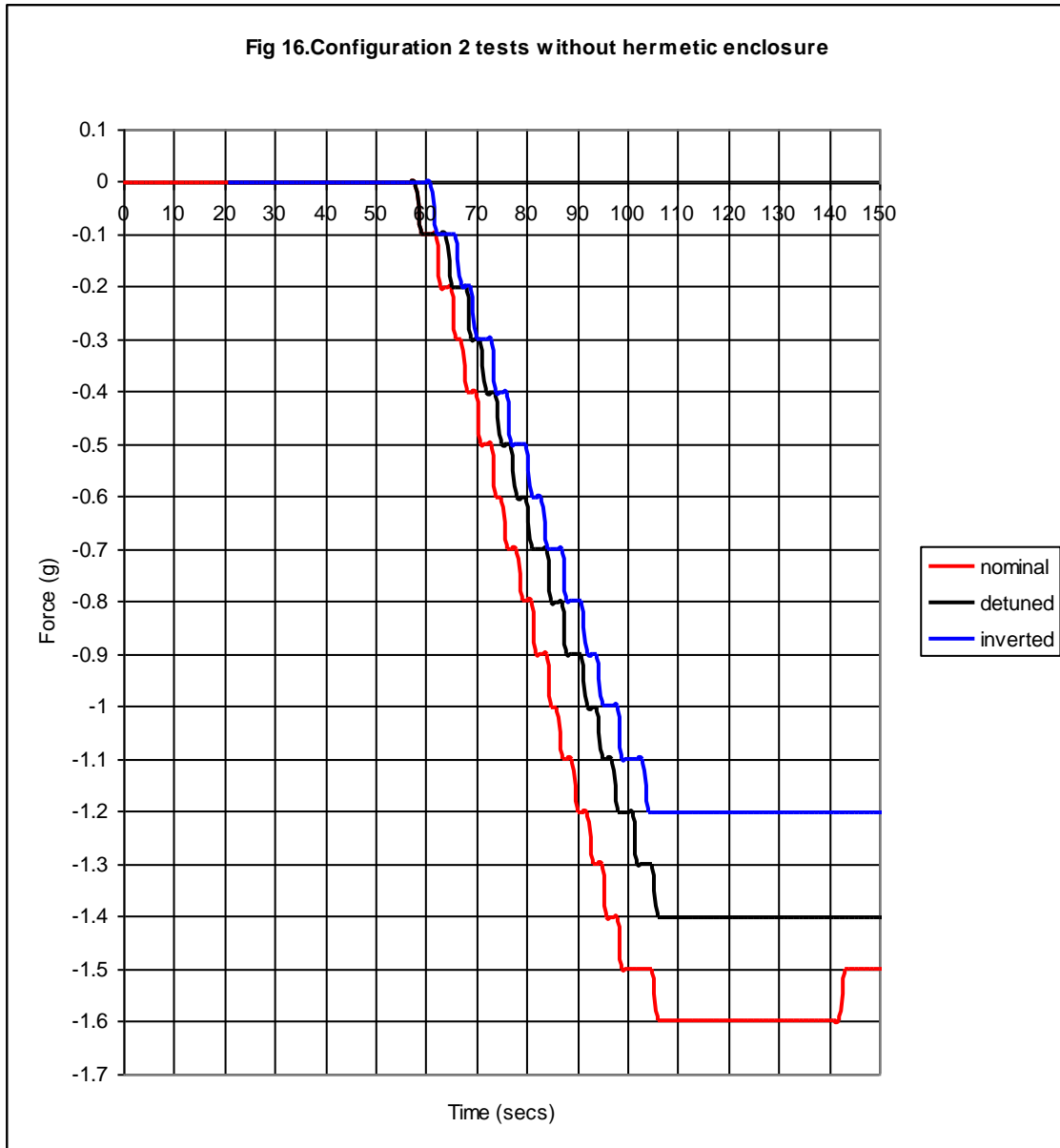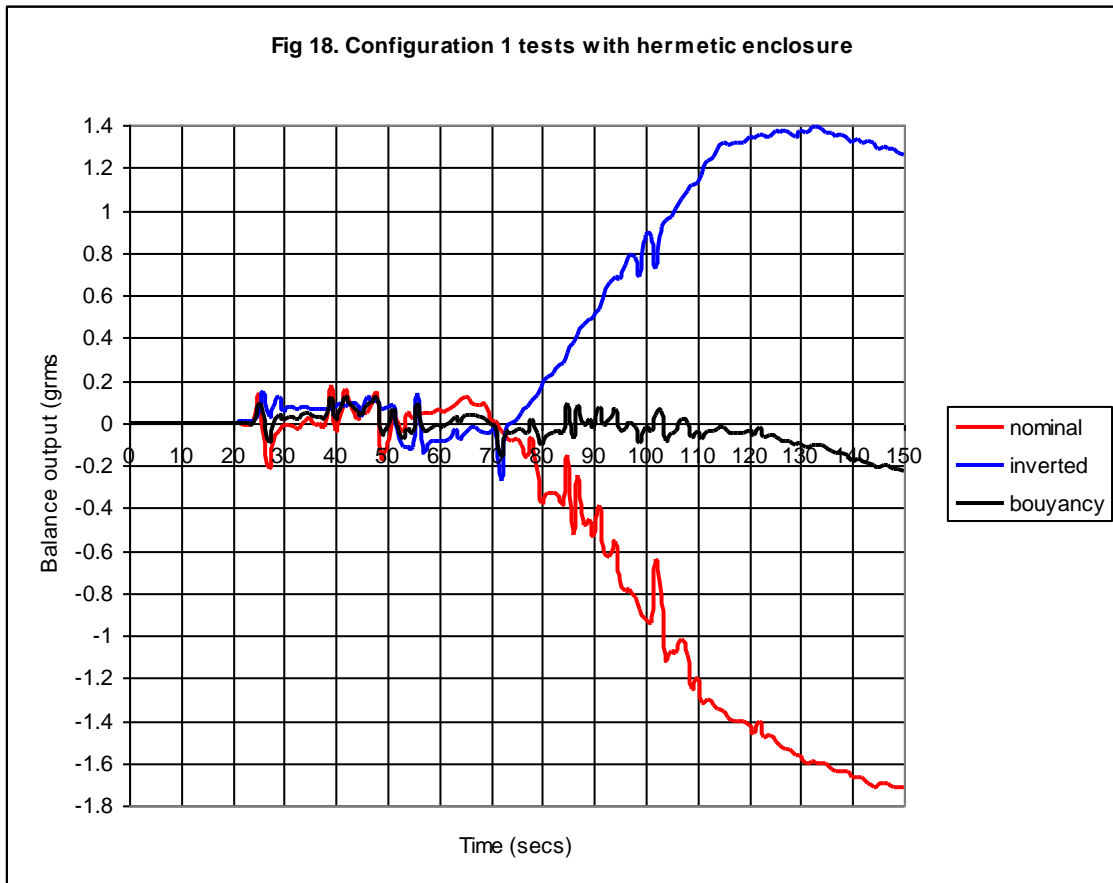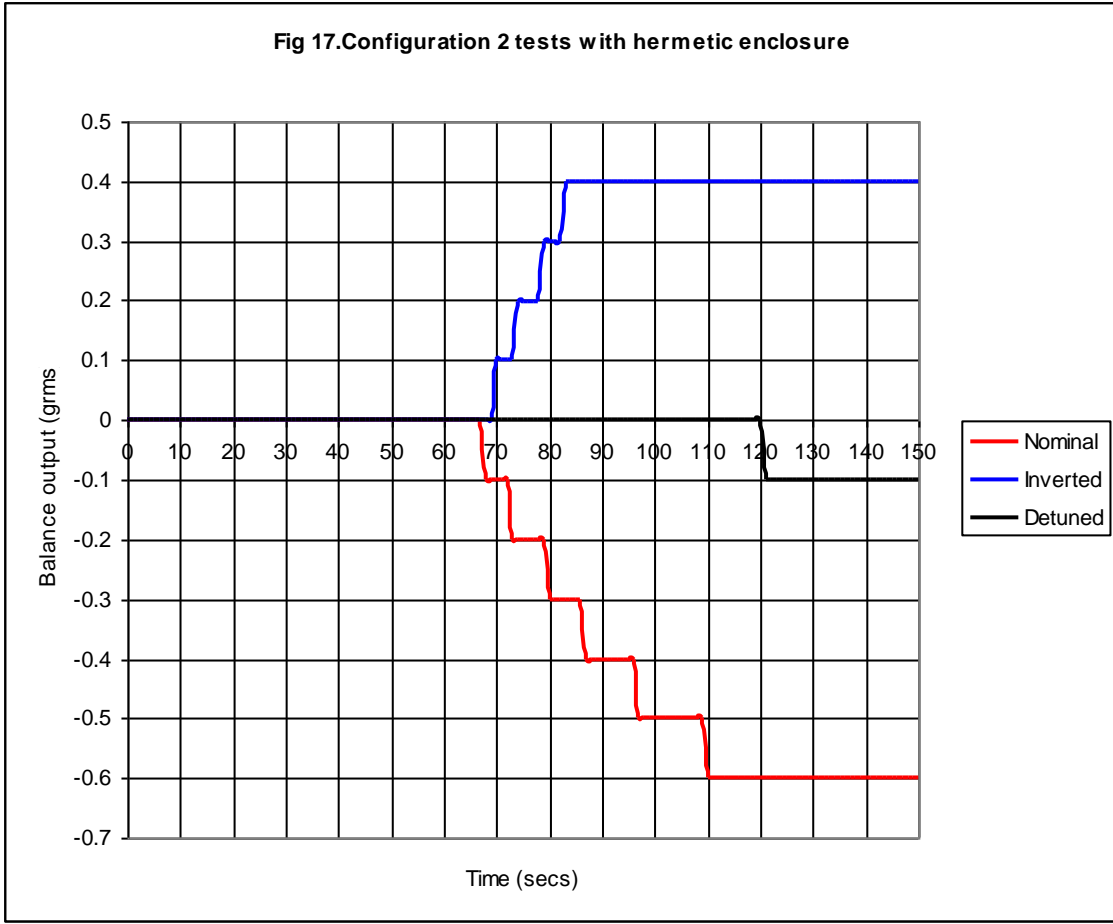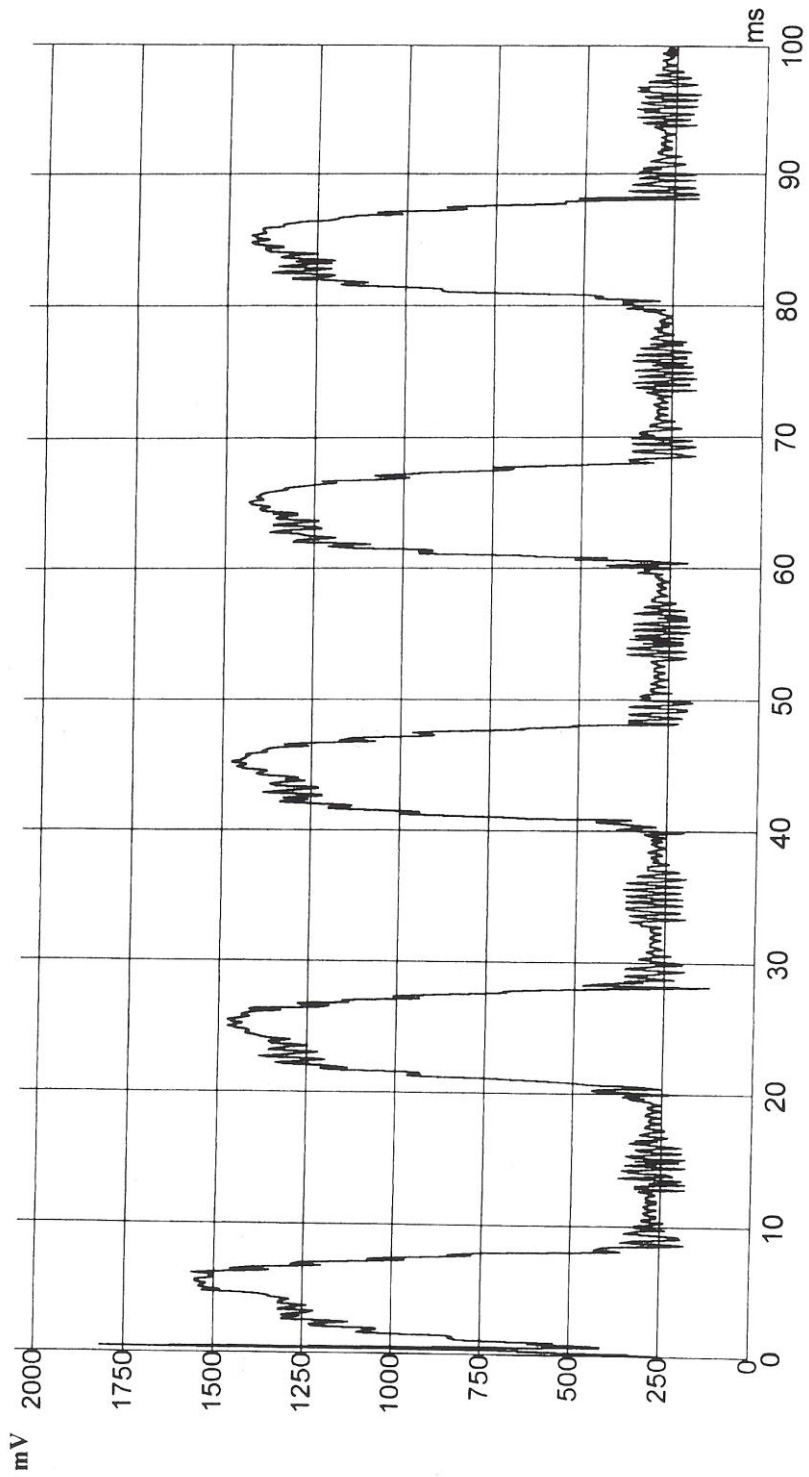
SPR Ltd

Fig 19.Power Detector Output.

SPR Ltd

SPR Ltd

Fig 20. Power & Thrust over 2 cycles

Fig 21. Predicted & Experimental Thrust

SPR Ltd

Fig 22.Configuration 1 responses for a constant spurious force

Fig 23. Configuration 2 responses for a constant spurious force

SPR Ltd

Fig 24. Predicted Response for Linear Spurious Forces

Fig 25. Predicted responses for Spurious pulsed force

SPR Ltd
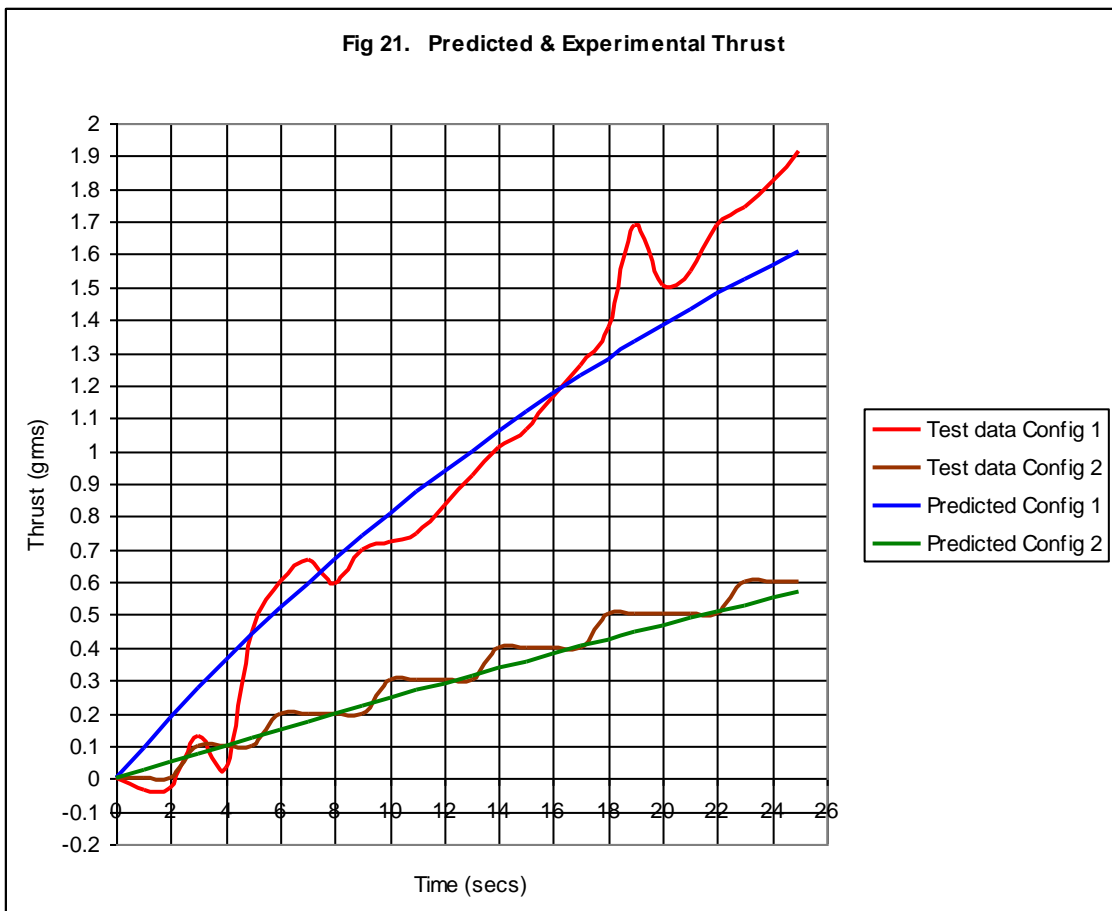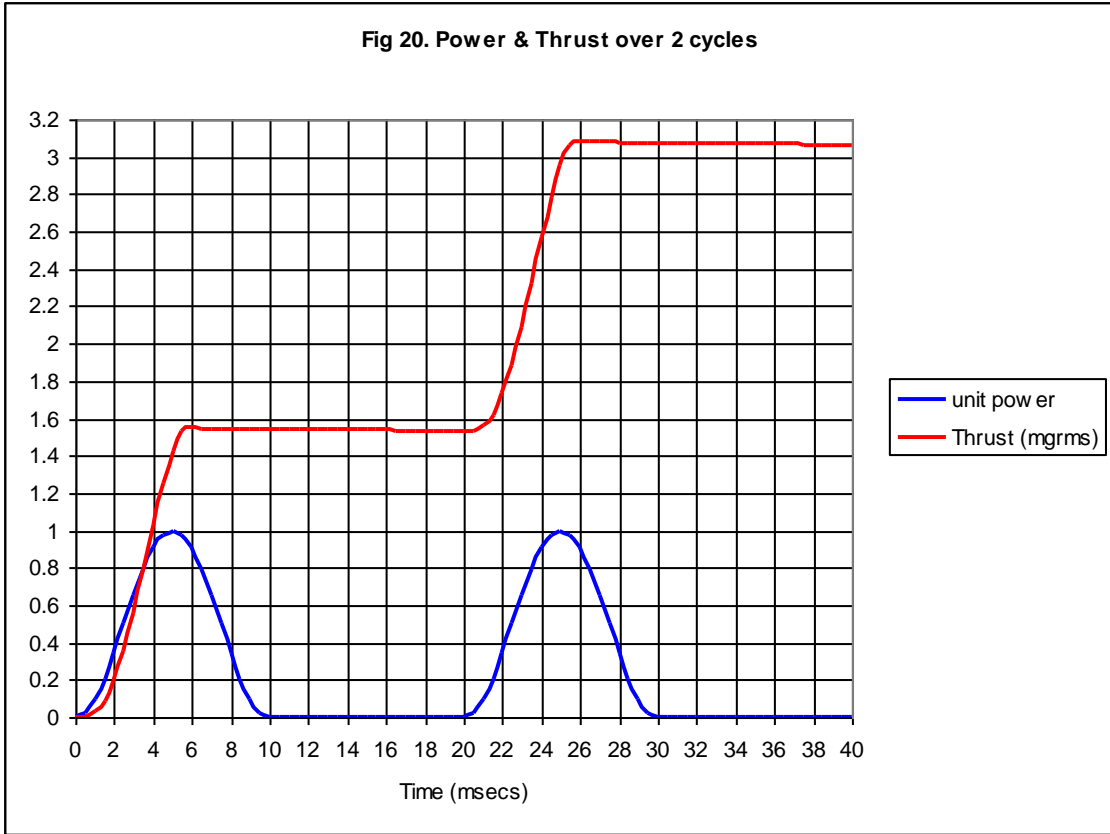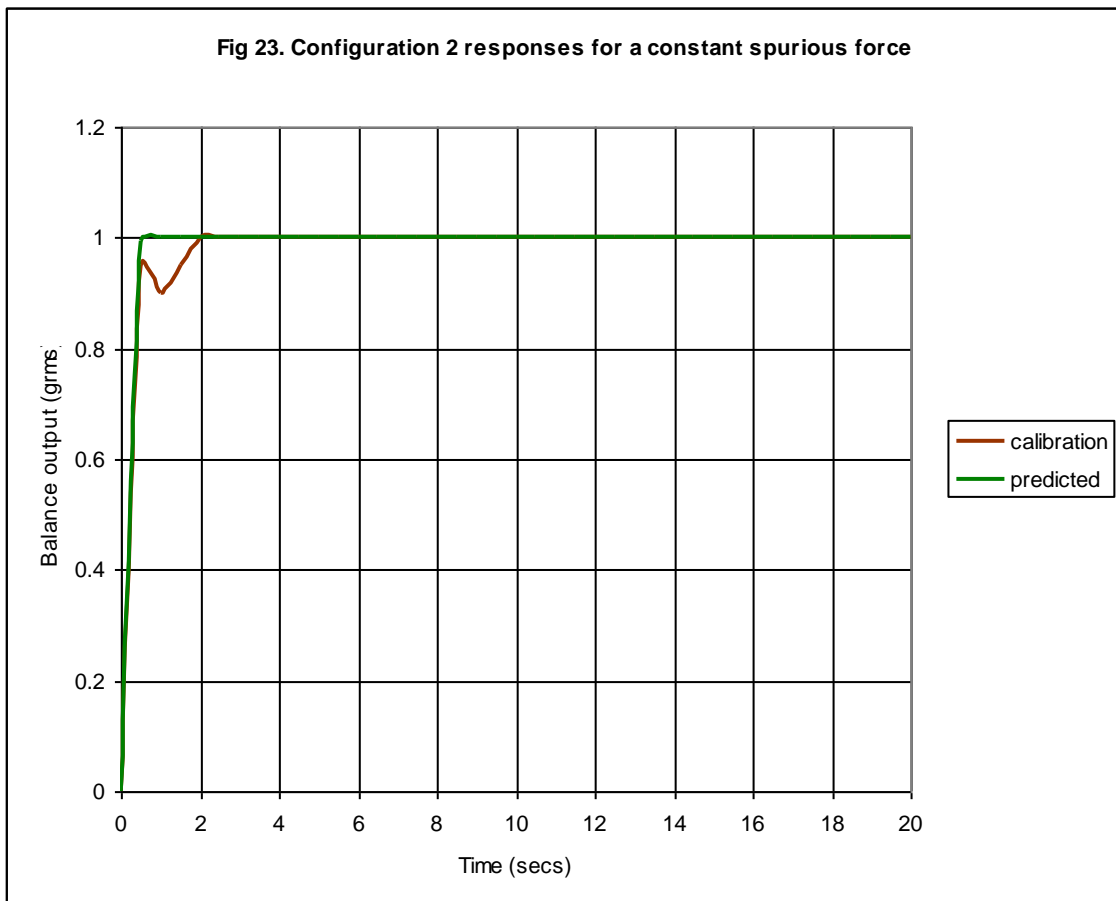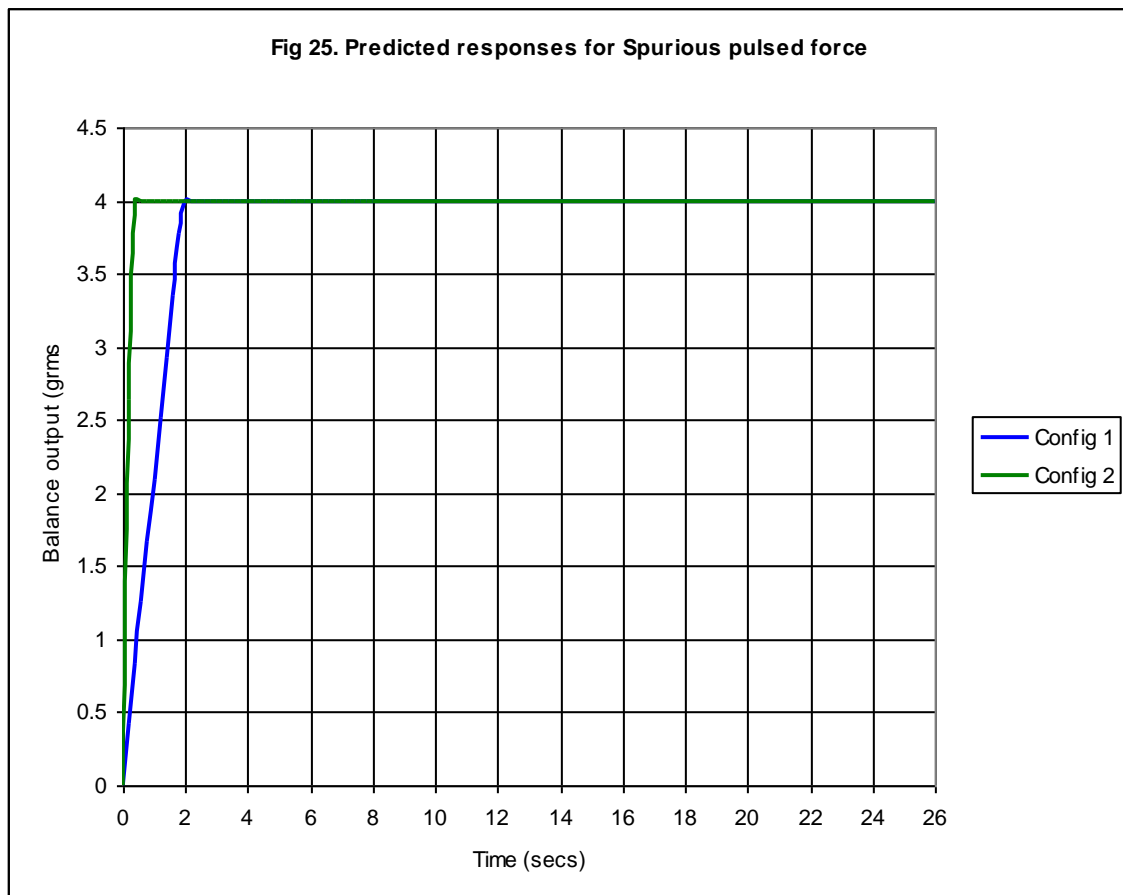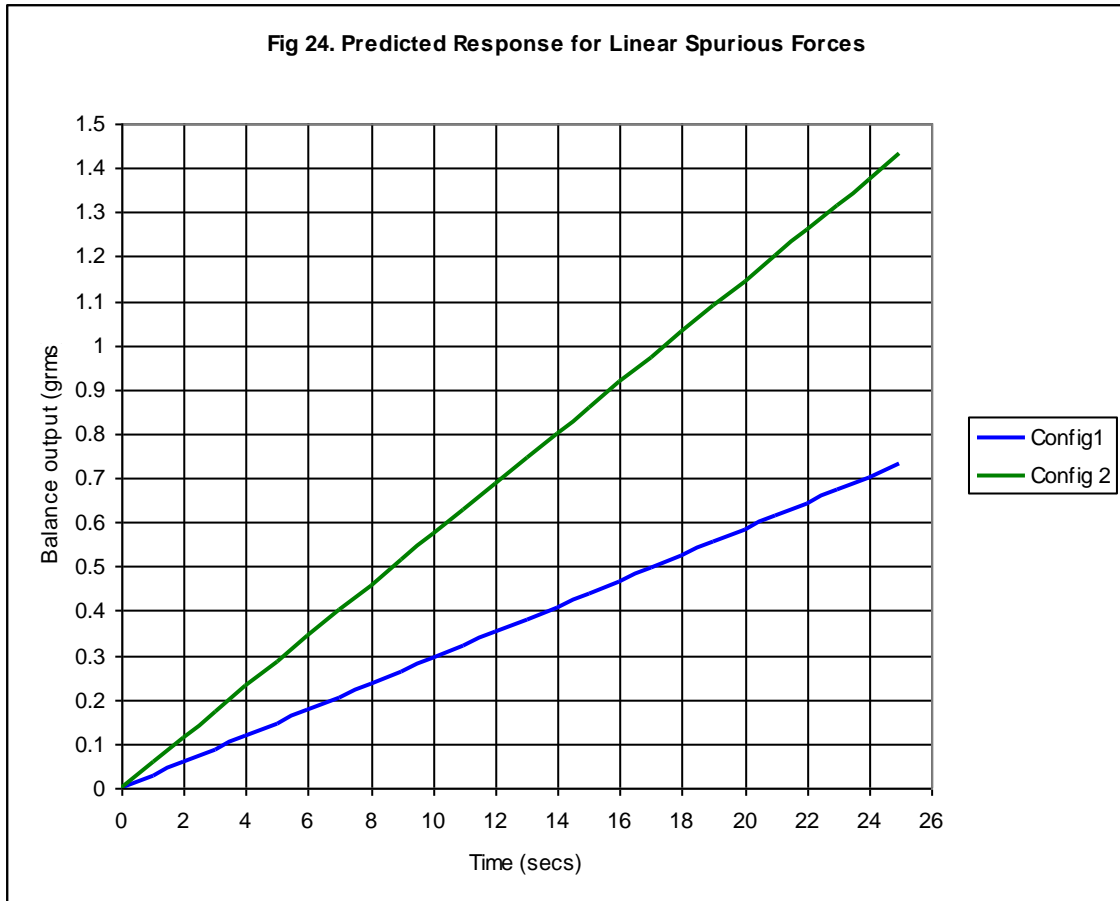
4.4 Pulse Measurements

As a final verification of the thrust profile theory given in section 4.3. an attempt was made to directly measure the pulsed thrust output on a digital oscilloscope. The load cell electronics were modified to include a two stage amplifier of gain 60×10^3 with ac coupling and low pass filtering. The thruster was tested using the original beam balance and load cell. The measured positive and negative response of this balance configuration are given in fig 26 together with the predicted response using the theoretical balance time constant.

The very high overall gain from load cell to oscilloscope(60×10^6) and the proximity of the high voltages (5kV) caused considerable EMC problems, particularly as the wanted data (thrust pulses) and the voltage transients were both at 50 Hz.

Three sets of measurements were taken, one with the thruster in nominal configuration and one in the inverted configuration.A further set was taken with additional counterbalance mass, so that the load cell was unloaded. This third test configuration gave a reference EMC response.
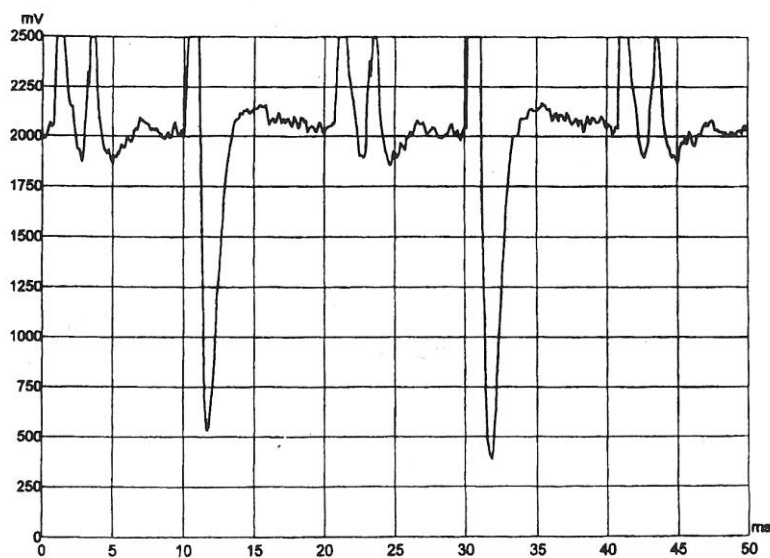
The oscilloscope traces for the three configurations are given in fig 27. Comparison with the power trace in fig 19 shows that the 'on' part of the cycle is characterised by a double positive EMC spike at the beginning and a single negative EMC spike at the end. These spikes were discounted and the remaining waveforms were then amplified and processed by subtracting the EMC response from the nominal and inverted responses. As the measurements were from ac coupled amplifier stages, the results were then integrated over two cycles to give the thrust output shown in fig 28.

Also given in fig 28 are the inverted and nominal thrust profiles predicted for the load cell balance configuration using equations 21 and 22. There is clear correlation between the predicted and measured thrust data over two cycles for both nominal and inverted configurations.
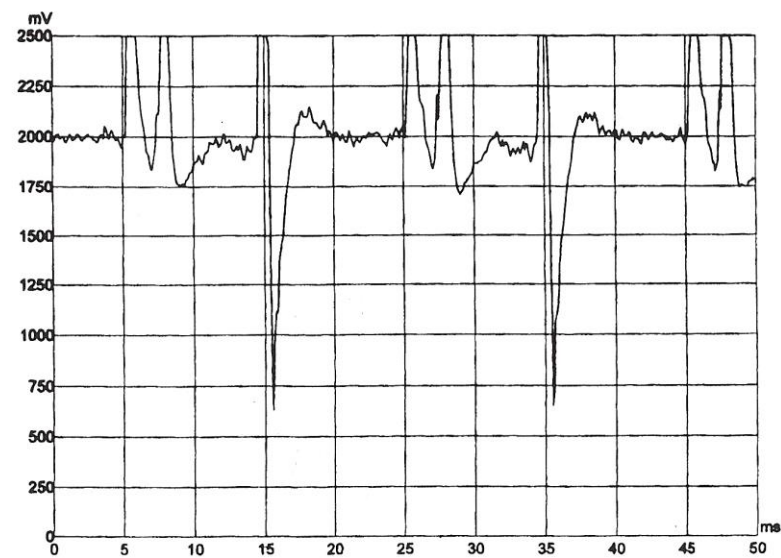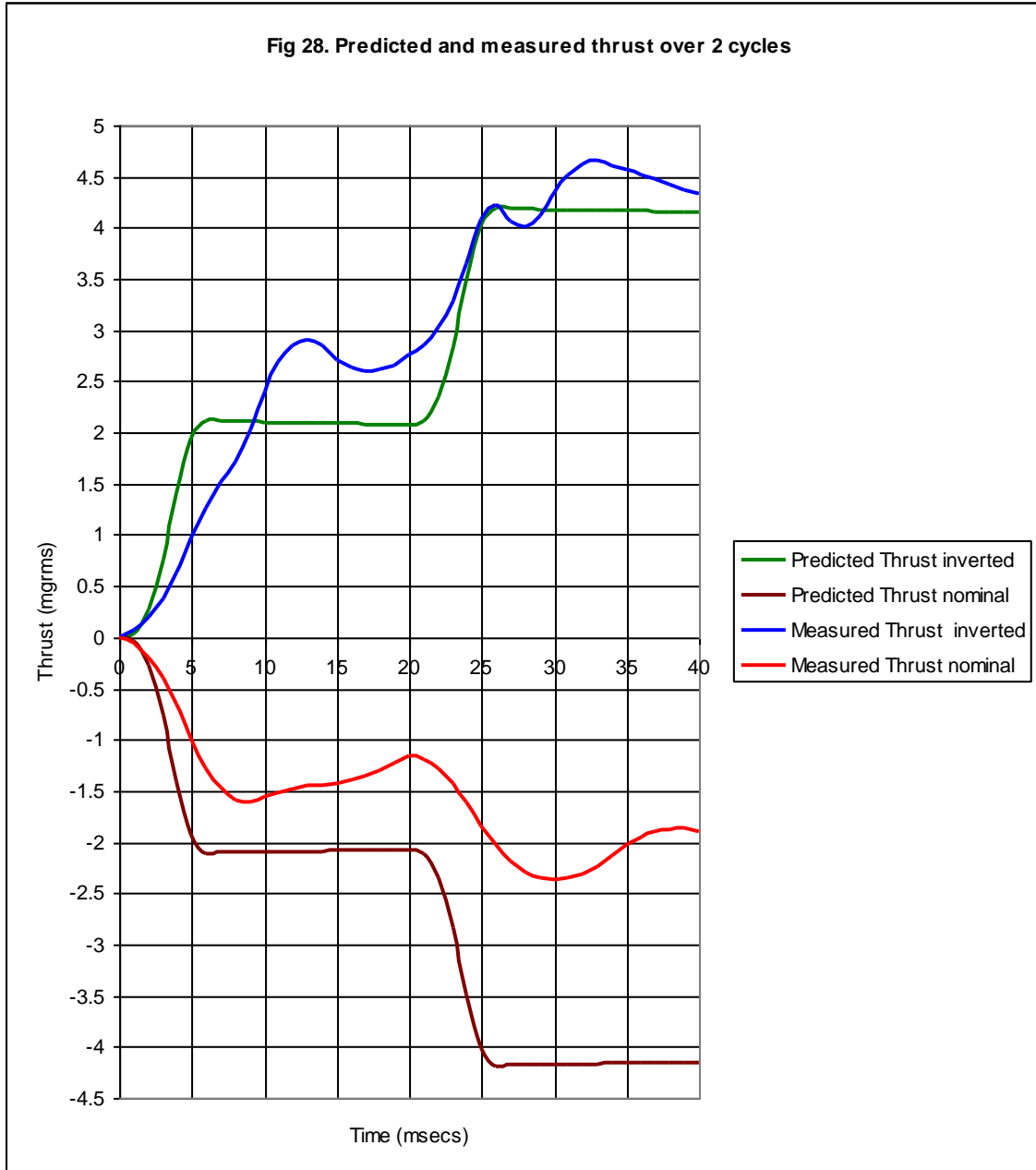
SPR Ltd

Fig 26.Predicted and measured responses for beam balance and load cell.
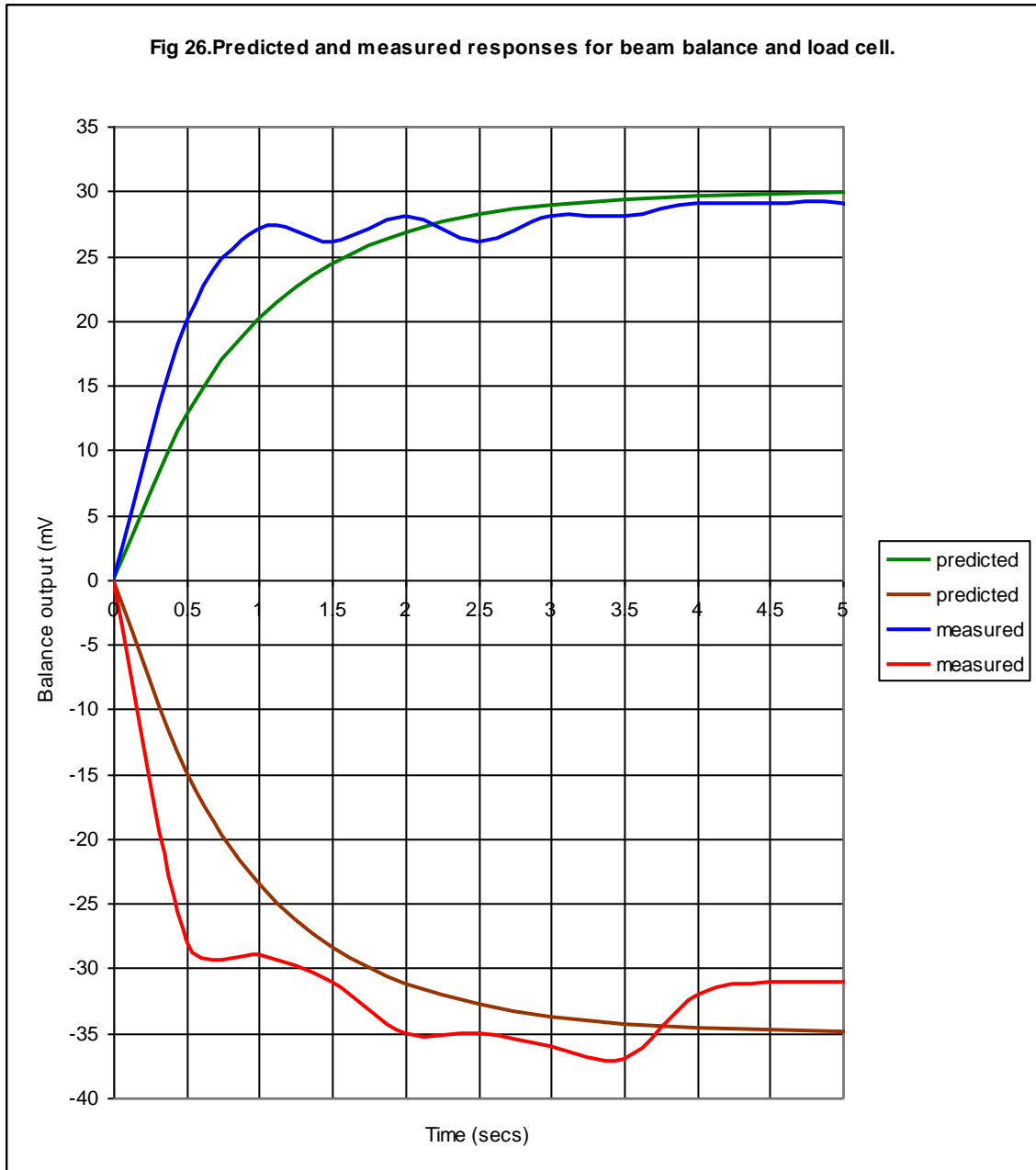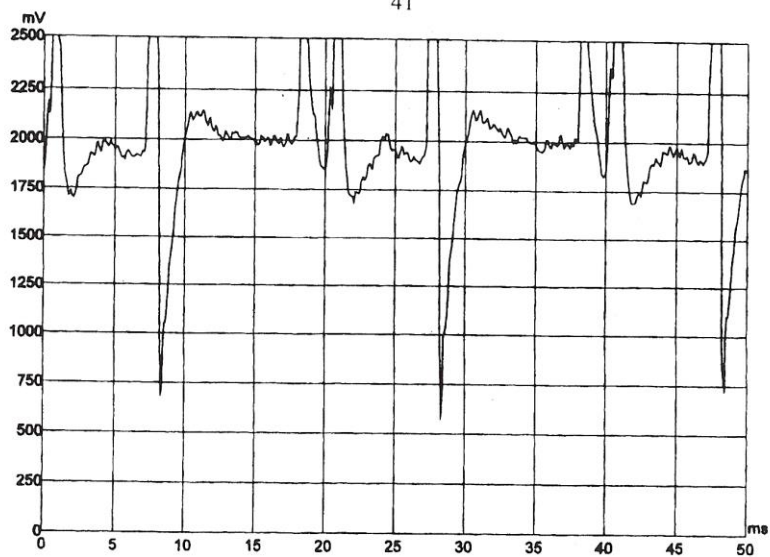
SPR Ltd

Nominal Configuration

Inverted Configuration

Reference EMC Configuration

Fig 27. Oscilloscope traces for pulse measurements.

SPR Ltd

SPR Ltd

Fig 28. Predicted and measured thrust over 2 cycles

SPR Ltd

5. Conclusions

- A theory has been developed for a propulsion technique which allows direct conversion from electrical energy at microwave frequencies to thrust.

- An expression has been developed to enable the thrust from such a system to be calculated.

- An experimental thruster was designed using a mathematical model to establish the basic dimensions and electrical characteristics.

- An experimental 850W thruster operating in S band was manufactured and resonant operation at microwave frequencies was tested using low power sources.

- The tuning dimensions for resonance at the nominal operating frequency of 2541 MHz and at the lower frequency limit of 2432 MHz were measured. These dimensions agreed closely with the tuning positions predicted by the model.

- A further test, short circuiting the dielectric section resulted in no resonance being detected, proving that propagation was taking place as designed.

- The experimental thruster was successfully powered from an 850W magnetron approximately 450 times over periods of up to 50 secs. A full range of thrust, power and temperature measurements were recorded. During the programme a total of 5 different magnetrons were used.

- The test programme included tests in both a nominal and an inverted position on three different balances. In all tests, when correctly tuned, the thruster gave an upward force in the nominal position and a downward force in the inverted position, in accordance with the design.

- Peak thrusts measured were comparable to those predicted from the theoretical expression.

- When not correctly tuned the thruster gave reduced thrust or no measurable thrust. Results over a range of input and resonance tuning adjustments gave good correlation between power and thrust measurements.

- The sequence in which test runs were carried out was shown to have no influence on the thrust measured.

- The operation of the cooling fan was shown to have no influence on the thrust measured.

SPR Ltd

- The direction of the outgassing of cooling air from the thruster was shown to have no influence on the thrust measured.

- The orientation with respect to the Earth's magnetic field was shown to have no influence on the thrust measured.

- Operation within a hermetic enclosure clearly demonstrated the reduction of the buoyancy offset due to the outgassing of cooling air.

- Expressions were derived for the thrust/time profile, to predict the pulsed thrust output, due to a half wave rectified voltage input to the magnetron.

- These expressions were used to predict the thrust/time profiles expected when the thruster was tested on two balances with widely different spring constants.

- The thrust/time profiles measured agreed closely with those predicted for both balances.

- Force/time profiles were predicted for assumed spurious forces due to mass change, thermal slopes and electromagnetic pulse forces. In each case the change in profile with the different balance configurations was opposite to the profile change actually measured. This finding totally confirms the earlier tests that eliminated these spurious forces.

- The thrust/time profile equations predicted a stepped thrust output when viewed over a number of pulse cycles. This stepped thrust output was measured using the processed output of an oscilloscope.

- The pulsed thrust output correlated closely with the predicted output in both nominal and inverted configurations.

- It is concluded that the test data presented verifies the theory of operation of the microwave thruster and thus, for the first time, a method of propulsion that does not rely on propellant has been demonstrated.

SPR Ltd